Mast cells mediate malignant pleural effusion formation

Anastasios D. Giannou,[1] Antonia Marazioti,[1] Magda Spella,[1] Nikolaos I. Kanellakis,[2] Hara Apostolopoulou,[1] Ioannis Psallidas,[1,3] Zeljko M. Prijovich,[1] Malamati Vreka,[1] Dimitra E. Zazara,[1] Ioannis Lilis,[1] Vassilios Papaleonidopoulos,[1] Chrysoula A. Kairi,[1,4] Alexandra L. Patmanidi,[2] Ioanna Giopanou,[1] Nikolitsa Spiropoulou,[1] Vaggelis Harokopos,[5] Vassilis Aidinis,[6] Dionisios Spyratos,[7] Stamatia Teliousi,[8] Helen Papadaki,[9] Stavros Taraviras,[2] Linda A. Snyder,[10] Oliver Eickelberg,[11] Dimitrios Kardamakis,[12] Yoichiro Iwakura,[13] Thorsten B. Feyerabend,[14] Hans-Reimer Rodewald,[14] Ioannis Kalomenidis,[4] Timothy S. Blackwell,[15] Theodora Agalioti,[1] and Georgios T. Stathopoulos[1,4,11,15]

[1]Laboratory for Molecular Respiratory Carcinogenesis, Department of Physiology, and [2]Stem Cell Biology Laboratory, Department of Physiology, Faculty of Medicine, University of Patras, Rio, Achaia, Greece. [3]Oxford Centre for Respiratory Medicine, Churchill Hospital, Oxford, United Kingdom. [4]First Department of Critical Care and Pulmonary Medicine, University of Athens School of Medicine, General Hospital Evangelismos, Athens, Attica, Greece. [5]Expression Profiling Unit and [6]Division of Immunology, Biomedical Sciences Research Center (BSRC) Alexander Fleming, Vari, Attica, Greece. [7]Department of Pulmonary Medicine, Hospital G. Papanikolaou, Faculty of Medicine, Aristotle University of Thessaloniki, and [8]Department of Cytology, Hospital G. Papanikolaou, Thessaloniki, Greece. [9]Department of Anatomy, Faculty of Medicine, University of Patras, Rio, Achaia, Greece. [10]Oncology Discovery Research, Janssen R&D LLC, Spring House, Pennsylvania, USA. [11]Comprehensive Pneumology Center (CPC), University Hospital, Ludwig-Maximilians University and Helmholtz Zentrum München, Member of the German Center for Lung Research (DZL), Munich, Germany. [12]Department of Radiation Oncology and Stereotactic Radiotherapy, Faculty of Medicine, University of Patras, Rio, Achaia, Greece. [13]Research Institute for Biomedical Sciences, Tokyo University of Science, Tokyo, Japan. [14]Division for Cellular Immunology, Deutsches Krebsforschungszentrum (DKFZ), Heidelberg, Baden-Württemberg, Germany. [15]Department of Medicine, Division of Allergy, Pulmonary and Critical Care Medicine, Vanderbilt University School of Medicine, Nashville, Tennessee, USA.

Mast cells (MCs) have been identified in various tumors; however, the role of these cells in tumorigenesis remains controversial. Here, we quantified MCs in human and murine malignant pleural effusions (MPEs) and evaluated the fate and function of these cells in MPE development. Evaluation of murine MPE-competent lung and colon adenocarcinomas revealed that these tumors actively attract and subsequently degranulate MCs in the pleural space by elaborating CCL2 and osteopontin. MCs were required for effusion development, as MPEs did not form in mice lacking MCs, and pleural infusion of MCs with MPE-incompetent cells promoted MPE formation. Once homed to the pleural space, MCs released tryptase AB1 and IL-1β, which in turn induced pleural vasculature leakiness and triggered NF-κB activation in pleural tumor cells, thereby fostering pleural fluid accumulation and tumor growth. Evaluation of human effusions revealed that MCs are elevated in MPEs compared with benign effusions. Moreover, MC abundance correlated with MPE formation in a human cancer cell–induced effusion model. Treatment of mice with the c-KIT inhibitor imatinib mesylate limited effusion precipitation by mouse and human adenocarcinoma cells. Together, the results of this study indicate that MCs are required for MPE formation and suggest that MC-dependent effusion formation is therapeutically addressable.

Introduction

Inflammation was recently recognized as an enabling hallmark of cancer that may mediate tumor growth and dissemination instead of tumor eradication (1). Inflammatory signaling networks in the tumor microenvironment can be initiated and orchestrated by malignant or immune cells; the networks conditionally facilitate tumor progression or regression depending on tumor type, immune effector cell type, and anatomic context (2–4). The identification of such inflammatory loops is of particular interest in the hunt for anticancer therapies that are anticipated to be more effective and less toxic than conventional chemotherapy (5).

In addition to macrophages, neutrophils, and lymphocytes, mast cells (MCs) were recently found to be recruited to pancreatic and other tumors and to facilitate tumor growth (6, 7). Although they are relatively sparse, MCs are appealing candidates for tumor promotion, since they can release a battery of mediators to orchestrate the tumor milieu (8–11). However, MCs were found to be tumor-protective or indifferent in other settings (12–14). While the reasons for the divergent MC functions in cancer are not known, new models of MC deficiency lend promise to solve this riddle (15, 16).

Malignant pleural effusion (MPE) is extremely common in patients with lung, breast, or other adenocarcinomas (17, 18). No treatment exists, and palliative attempts may cause further morbidity and mortality (19, 20). MPE was recently reclassified as a separate stage of lung cancer, since it was acknowledged to represent a distinct form of metastatic disease with very short survival (18, 21, 22). Simultaneously, we and others used mouse models to hypothesize that MPE is primarily an immune- and vascular-

Authorship note: Timothy S. Blackwell, Theodora Agalioti, and Georgios T. Stathopoulos are co–senior authors.
Conflict of interest: Linda A. Snyder is an employee of Janssen R&D LLC, the manufacturer of anti-CCL2 and anti-CCL12 Abs.
Submitted: November 14, 2014; **Accepted:** March 26, 2015.
Reference information: *J Clin Invest*. 2015;125(6):2317–2334. doi:10.1172/JCI79840.

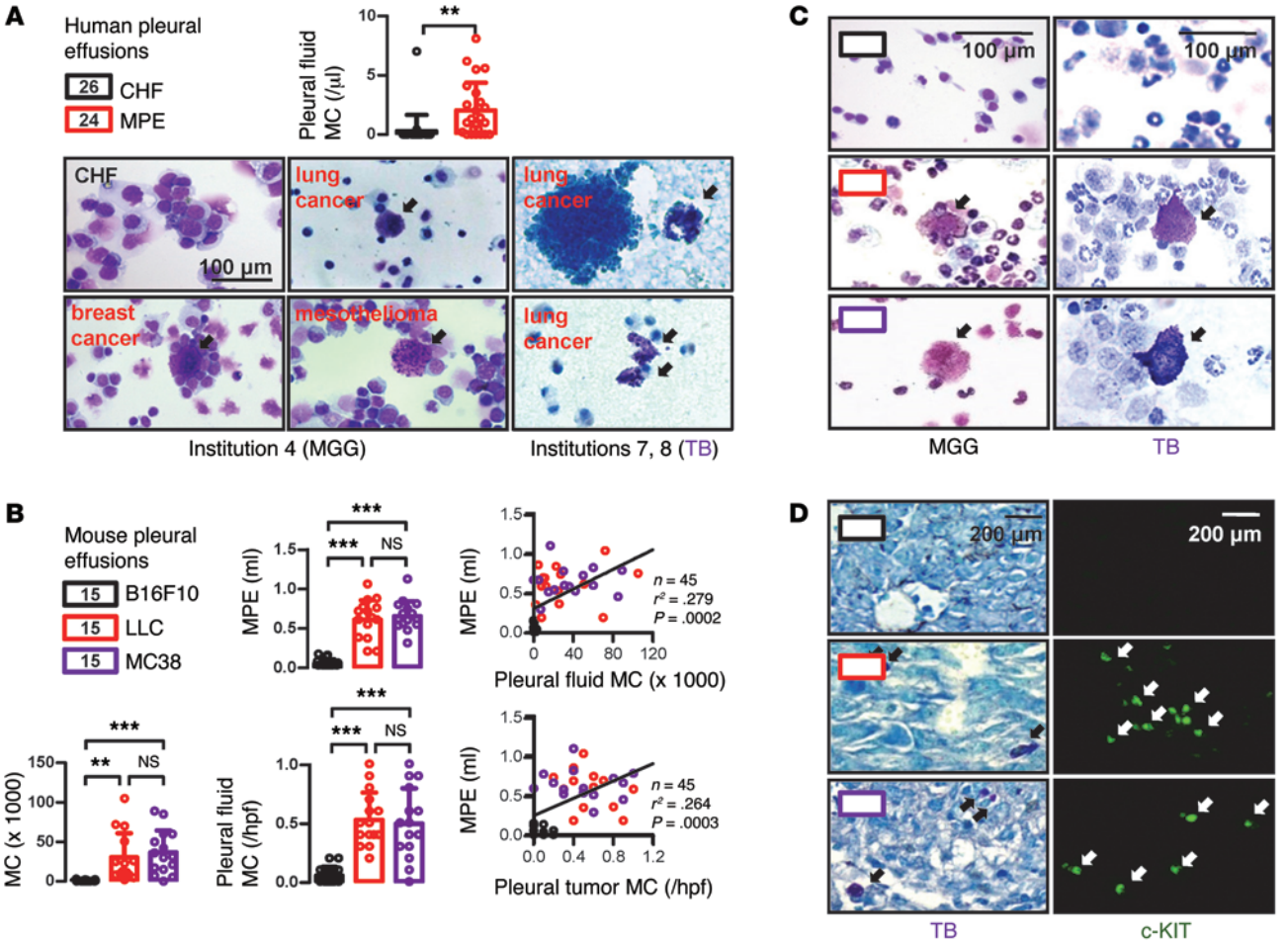

Figure 1. MCs in human and murine MPEs. (**A**) Pleural MCs from patients with MPEs (n = 24) or CHF (n = 26) from 2 Hellenic hospitals. (**B**) MPEs and MCs of C57BL/6 mice 14 days after pleural delivery of 1.5 × 10^5 syngeneic tumor cells (n = 15 mice per tumor cell type). Right: correlation between MPE and tumor-MC abundance and MPE volume, with linear regression line, sample size (n), probability value (P), and squared Pearson correlation coefficient (r^2). Hpf, high-power field. (**C** and **D**) Representative microphotographs of pleural fluid (**C**) and tumor (**D**) MCs from mice from **B**. Data presented as data points, mean ± SD. Numbers in boxes indicate sample size. Arrows indicate MCs. NS, $P > 0.05$; $^{**}P < 0.01$; and $^{***}P < 0.001$, by 2-tailed Student's t test (**A**) or 1-way ANOVA with Bonferroni post hoc tests (**B**).

mediated manifestation of pleural-metastasized cancers (23, 24). However, the immune cells that drive MPE remain unidentified.

Here we describe the discovery of MCs in human and mouse MPEs and the elucidation of their fate and role. We show that MCs are driver cells required for MPEs and uncover the key messengers that instate tumor-MC circuitry during MPE development. Importantly, we provide proof-of-concept data supporting that MC-dependent MPEs are targetable using existing drugs; these data lend promise for translational applications of our findings.

Results

MCs in MPEs. MCs were encountered on May-Gruenwald-Giemsa–stained (MGG-stained) archival specimens of human MPEs from our pleural patient biobank. To rule out a local artifact, MCs were verified on metachromatic toluidine blue–stained (TB-stained) MPE samples from a different hospital. Systematic evaluation of samples and data from our pleural patient biobank revealed substantial MC numbers (millions/cavity) in MPEs that were significantly elevated compared with benign effusions from congestive heart failure (CHF; Figure 1A). Increased MC numbers were also identified in 2 different mouse models of MPEs that develop 14 days after intrapleural delivery of syngeneic Lewis lung carcinoma (LLC; 30,310 ± 30,440 MC/cavity) or MC38 colon (36,590 ± 27,690 MC/cavity adenocarcinoma) cells (25, 26), compared with controls injected with MPE-incompetent B16F10 melanoma cells (999 ± 1,008/cavity) or saline (755 ± 384/cavity; n = 3). In addition, MC abundance was correlated with the volume of experimental effusions (Figure 1B). MPE MCs displayed typical morphology and TB/c-KIT staining, but they were easily overlooked when MGG, Wright, or other conventional staining was employed (Figure 1, C and D, and Figure 2A). MPE MCs were identified as $CD45^+c\text{-}KIT^+Sca1^+Lin^-$ by flow cytometry (27–29), were reduced in c-KIT–defective $c\text{-}Kit^{Wsh}$ mice (30), and were completely absent from MC-eradicated $Cpa3^{Cre/+}$ mice (15) — a mouse model of more complete and selective MC deficiency as compared with $c\text{-}Kit^{Wsh}$ mice — that were challenged with pleural adenocarcinoma cells (Figure 2B). In mice with MPEs, MCs were preferentially located in

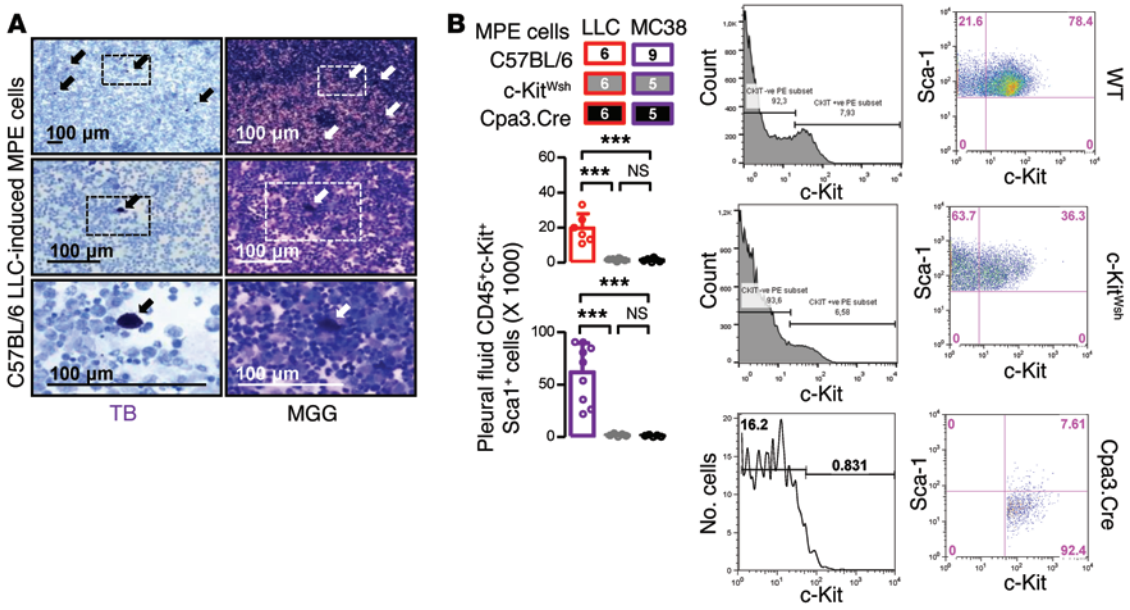

Figure 2. Characterization of MCs from mouse MPEs. (**A**) Representative pleural cell staining from mice from Figure 1B: MCs (arrows) were clearly discernible by TB, but not by routine stains. Each image represents a magnification of the inlay from the image above. (**B**) Flow cytometry gating and data summary of adenocarcinoma-induced MPEs from C57BL/6 (n = 15), *c-Kit*^{Wsh} (n = 11), and *Cpa3*$^{Cre/+}$ (n = 11) mice. Data presented as data points, mean ± SD. Numbers in boxes indicate sample size. Arrows indicate MC. NS, $P > 0.05$; ***$P < 0.001$ by 1-way ANOVA with Bonferroni post hoc tests.

parietal and mediastinal, but not visceral, pleural tumors; most commonly resided in viable, but not necrotic, tumor tissue; and aggregated near or at the tumor front, forming chains or clusters (Figure 3). Hence, pleural MC accumulation is associated with MPE development in humans and mice. Moreover, MPE MCs appear to stream into the malignancy-affected pleural space via the parietal and mediastinal pleural surfaces.

Dynamic MC accumulation in the pleural space. To test MC kinetics during MPE development, we cultured murine BM-derived MCs (BMMCs) using c-KIT ligand (KITL) and interleukin-3 (IL-3), according to previously published protocols (31). BMMCs of C57BL/6 mice stained TB$^+$ (>90%), CD45$^+$c-KIT$^+$Sca1$^+$Lin$^-$ (>80%), and CD25$^+$ (>50%) — and BMMCs of red-fluorescent *mT/mG* mice (32) — formed pseudopodia and moved, confirming the nature of these cells (Figure 4, A–C, and Supplemental Videos 1 and 2; supplemental material available online with this article; doi:10.1172/JCI79840DS1). BMMCs of luminescent CAG-luc-EGFP mice (33) emitted light proportional to cell number, and BMMCs of green fluorescent CAG-EGFP mice (34) were green fluorescent (Figure 4, D and E). When pulsed i.v. into irradiated C57BL/6 recipients adoptively reconstituted with *c-Kit*^{Wsh} BM (35), these tracer BMMCs distributed diffusely. However, when chimeras were challenged exclusively with pleural adenocarcinoma cells, BMMCs accumulated in the thorax concomitant with MPEs (Figure 5, A and B). Similar results were obtained with nonirradiated *c-Kit*^{Wsh} mice pulsed s.c. with tracer BMMCs (Figure 5C). Hence, pleural adenocarcinomas remotely mobilize/recruit MCs via circulating messengers.

CCL2 as an adenocarcinoma-derived mastokine. To identify these messengers, effusion-competent and effusion-incompetent tumor cells were transcriptionally profiled on 2 different occasions (biological n = 2) by microarray analysis. Although 39 genes were overrepresented in MPE-competent adenocarcinoma cells on both occasions, only 2 RNAs possessed cytokine/chemokine activity required for systemic MC recruitment and were selected for further study: *Spp1* and *Ccl2* (encoding osteopontin, or secreted phosphoprotein 1 [SPP1], and CCL2, respectively; Figure 6A and Supplemental Tables 1 and 2). ELISA of tumor cell–conditioned media (CM) validated the microarray, and serum ELISA of pleural tumor–bearing C57BL/6 mice identified a significant difference in serum CCL2, but not SPP1, between adenocarcinoma- and melanoma-bearing mice (Figure 6, B and C). In modified mastotaxis assays (36), tracer BMMCs migrated toward LLC cells expressing random and anti-*Spp1* shRNA (sh), but not toward B16F10 cells or LLC cells expressing sh*Ccl2* (Figure 6D and Figure 7A), implicating CCL2 in MPE-directed mastotaxis. Indeed, forced expression of *Ccl2* plasmid (p) in B16F10 cells restored, and forced expression of sh*Ccl2* in LLC cells inhibited, MPE (25) and MC accumulation. (Figure 7, B and C). Moreover, treatment of mice harboring pleural LLC cells with i.p. CCL2- and/or CCL12-neutralizing Ab (37) blocked MPE (38) and MC accumulation, and direct pleural-delivered recombinant mouse (rm) CCL2 attracted MCs (Figure 7, D–F). Finally, CCL2 (but not SPP1) levels were correlated with MC abundance in human MPEs (Figure 7G). Collectively, these data indicated that CCL2 is a key tumor-secreted MC attractant to the pleural space.

MCs are required for MPEs. We next investigated MC effects on effusion formation. Pleural co-delivery of BMMCs facilitated induction of MPE by B16F10 cells, which are naturally MPE incompetent, without fully instilling the phenotype of adenocarcinoma cells (Figure 8A). Vice versa, both *c-Kit*^{Wsh} and *Cpa3*$^{Cre/+}$

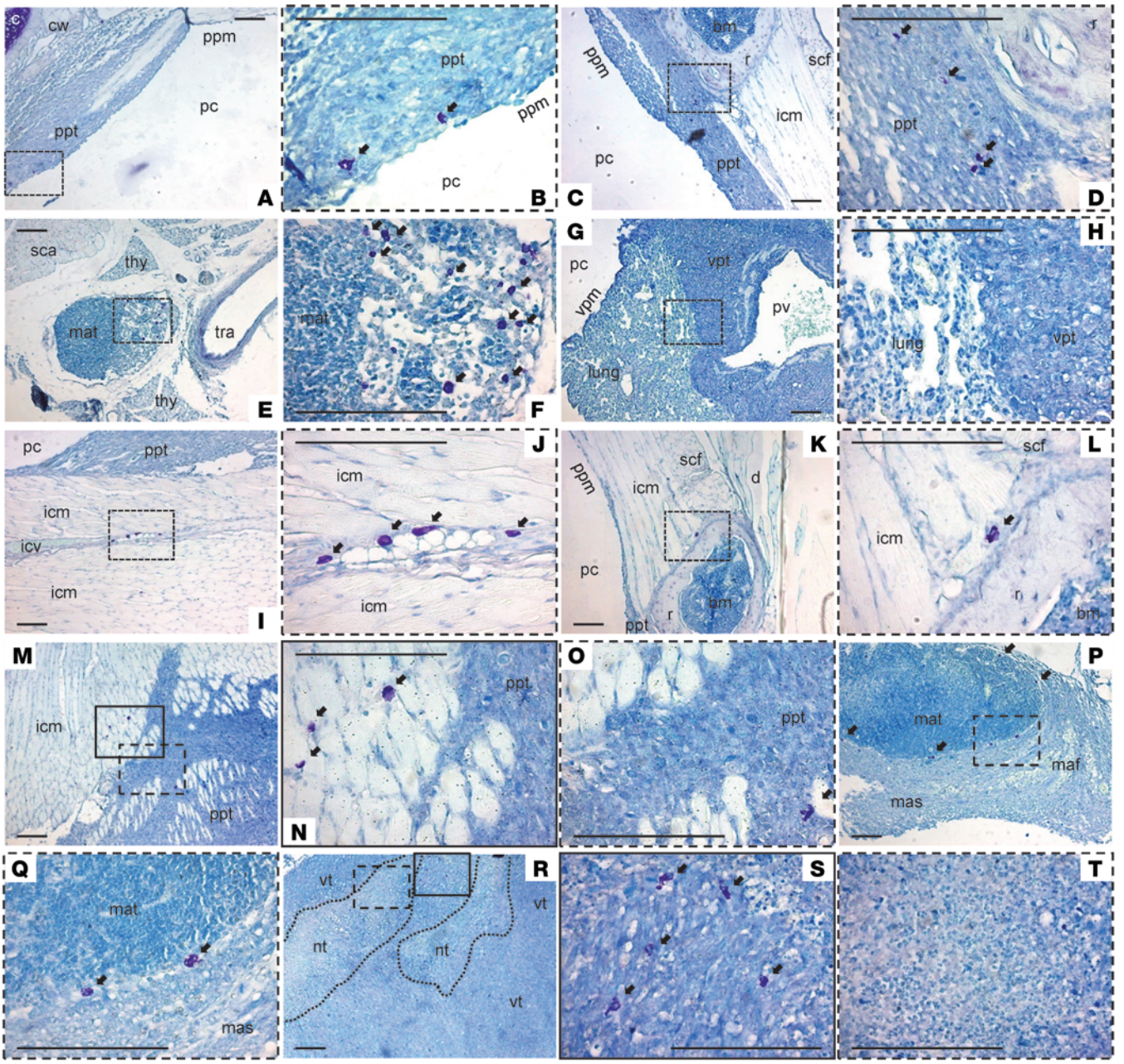

Figure 3. MC topology in experimental MPEs. Whole thoracic sections from mice with pleural tumors and effusions induced by LLC and MC38 adenocarcinomas stained with TB. MCs (arrows) were found in parietal pleural tumors (ppt) and mediastinal tumors (mat), but not in visceral pleural tumors (vpt) (**A**–**H**). MCs appeared to stream in from intercostals vessels, sequentially invading intercostal tissues (fat and muscle) and ppt, forming chains invading into tumors or rings strategically positioned around tumors (**I**–**Q**). MCs were exclusively located in viable (vt), but not necrotic (nt), tumor tissues (**R**–**T**). All scale bars = 300 μm. **B**, **D**, **F**, **H**, **J**, **L**, **N**, and **O**, **Q**, and **S** and **T**: magnified inlays from **A**, **C**, **E**, **G**, **I**, **K**, **M**, **P**, and **R**, respectively. c, rib cartilage; cw, chest wall; ppm, parietal pleural mesothelium; pc, pleural cavity; bm, rib BM; scf, subcutaneous fat; icm, intercostal muscle; thy, thymus; sca, scalene muscle; tra, trachea; vpm, visceral pleural mesothelium; pv, pulmonary vein; icv, intercostal vein; d, dermis; r, rib; maf, mediastinal fat; mas, mediastinum.

mice were protected against MPEs induced by both LLC and MC38 adenocarcinomas (Figure 8, B and C). In addition to MPE accumulation, MC deficiency resulted in retardation of pleural tumor growth, evident macroscopically (Figure 8, B and C), but also by decreased proliferating cell nuclear antigen (PCNA) immunoreactivity (Figure 8D). Since c-KIT is important for non-hematopoietic cells, too, we tested whether MCs are responsible for the phenotype of *c-Kit*^{Wsh} mice. Indeed, donor genotype determined the susceptibility of irradiated C57BL/6 or *c-Kit*^{Wsh} recipients reconstituted with C57BL/6 or *c-Kit*^{Wsh} BM (39) to LLC-triggered MPEs (Figure 8E). Consistent with prior reports, *c-Kit*^{Wsh} mice with pleural tumors were MC-poor (40), whereas *Cpa3*$^{Cre/+}$ mice were MC-eradicated (Figure 8, B and C). Indeed, BMMCs that stained TB$^+$ (>90%), CD45$^+$c-KIT$^-$Sca1$^+$ (>80%), Lin$^+$ (>40%), and CD25$^+$ (>80%) were derivable by IL-3/KITL culture from *c-Kit*^{Wsh} mouse BM (Figure 8F), resembling

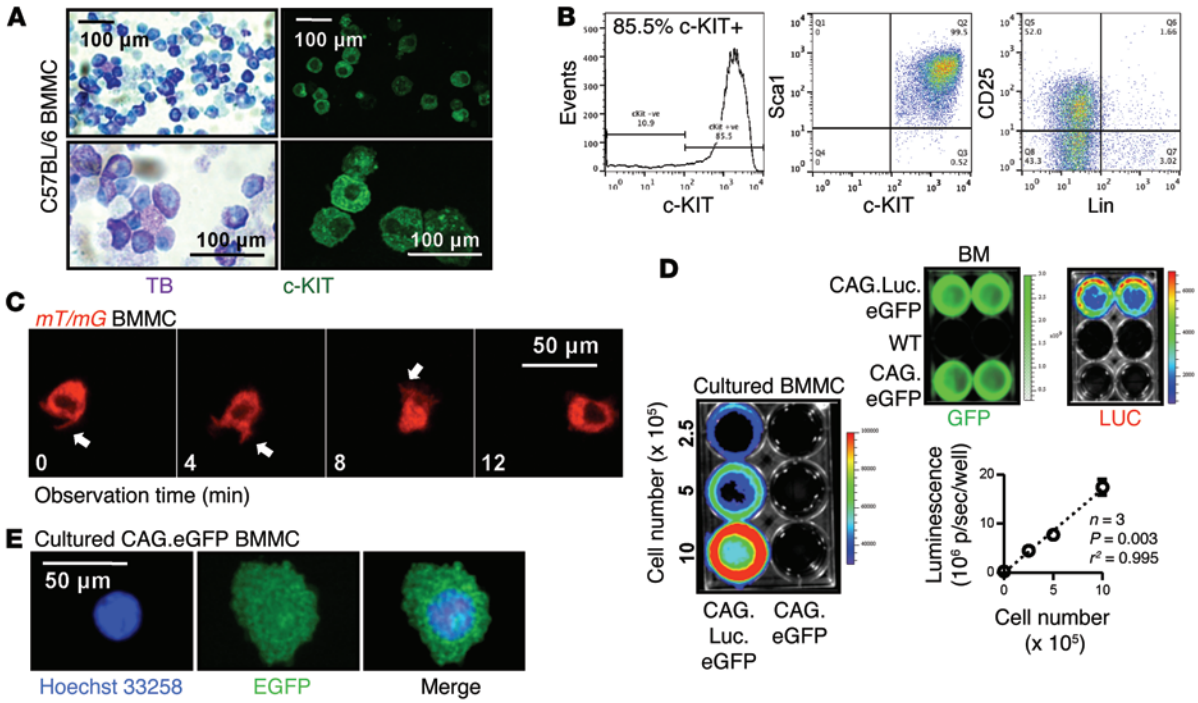

Figure 4. Isolation and characterization of BMMCs. (**A** and **B**) TB and c-KIT staining (**A**) and flow cytometry (**B**) of BMMCs. (**C**) Time-lapse imaging of *mT/mG* BMMCs extending pseudopodia (arrows) and moving at 0.25 mm/hour (see Supplemental Videos 1 and 2). (**D**) Luminescence and fluorescence images of BMMCs from C57BL/6, *CAG-luc-EGFP*, and *CAG-EGFP* mice. Scatterplot: Pearson correlation between luminescence and *CAG-luc-EGFP* BMMC number, with linear regression line, sample size (n = 3), probability value (P), and squared correlation coefficient (r^2). Data presented as mean ± SD. (**E**) *CAG-EGFP* BMMCs stained with nuclear dye.

MC-like innate immune cells described previously (29). We also sought to compare the relative contributions of MCs with those of macrophages during MPE development, since macrophages are the predominant cellular population in MPEs and are also chemoattracted to the pleural space by tumor-derived CCL2 (23, 25). For this, mice expressing *Cre* recombinase under the drive of the *Lyz2* promoter were crossed with mice expressing *Diphtheria* toxin selectively in somatic cells that undergo *Cre*-mediated recombination to generate a macrophage ablation model (*Lyz2-Cre* and *R26-DTA*, respectively; refs. 41, 42). Pleural macrophages of naive C57BL/6 mice were predominantly F4/80$^+$ and CD11b$^+$, but not CD11c$^+$; F4/80$^+$CD11b$^+$ pleural cells were markedly diminished in *Lyz2-Cre R26-DTA* mice compared with single transgenic controls (Figure 9A). Interestingly, *Lyz2-Cre R26-DTA* mice were protected against MPEs induced by both LLC and MC38 adenocarcinomas to a degree comparable to both mouse models of MC deficiency (Figure 9B). Hence, MCs are required for effusion formation, and they are equally important with much more prevalent cell types, such as macrophages. In addition, *c-Kit*^{Wsh} and *Cpa3*$^{Cre/+}$ mice can serve as tumor models of MC depletion and eradication, respectively.

Tumor-secreted osteopontin causes MC degranulation. We next examined the role of tumor-originated osteopontin (encoded by the *SPP1* gene in humans and the *Spp1* gene in mice) — the other candidate detected by tumor cell microarray — in MC-dependent effusions. We had previously identified that SPP1 is a marked mediator of vascular permeability that leads to MPE accumulation (43). In addition to its vasoactive effects, we determined here in multiple ways that tumor-secreted SPP1 promoted MC activation and degranulation. Adenocarcinoma cell-CM caused SPP1-dependent BMMC degranulation, and rmSPP1 directly degranulated BMMCs (Figure 10 and Supplemental Video 3). SPP1 effects were only partial, indicating the presence of additional tumor-elicited players in MC activation. Collectively with our past work, these data established dual functions of tumor-derived SPP1 during effusion development: in addition to inducing vascular leakage, osteopontin degranulates MCs.

Adenocarcinoma-primed MCs secrete tryptase AB1 and IL-1β to foster MPEs. To identify how pleural adenocarcinoma–recruited and pleural adenocarcinoma–primed MCs mediate effusion development, 2 different BMMC cultures were exposed to tumor-CM and were profiled transcriptionally (biological n = 2). Four BMMC transcripts were induced specifically and consistently by adenocarcinoma-CM, including secretory genes *Tpsab1* and *Il1b* and membrane/granule-associated *Cd68* (Figure 11A and Supplemental Tables 3–5). Indeed, adenocarcinoma-CM caused IL-1β release by BMMCs in a SPP1-dependent fashion, and adenocarcinoma-induced MPEs featured substantial IL-1β levels, which were reduced in *c-Kit*^{Wsh} mice (Figure 11, B and C). Staining of *C57BL6* BMMC and MPE cells for IL-1β, c-KIT, CD68, and the granule tag avidin localized IL-1β both in granules and the cytoplasm, and identified that c-KIT$^+$CD68$^+$ MCs are a subset of IL-1β–expressing cells in MPEs (Figure 11, D-F). Importantly, *Il1b*$^{-/-}$ mice (44) were protected from MPEs induced by LLC cells, similar to *c-Kit*^{Wsh} and *Cpa3*$^{Cre/+}$ mice. In multiple MC reconstitution experiments, C57BL/6 — but not

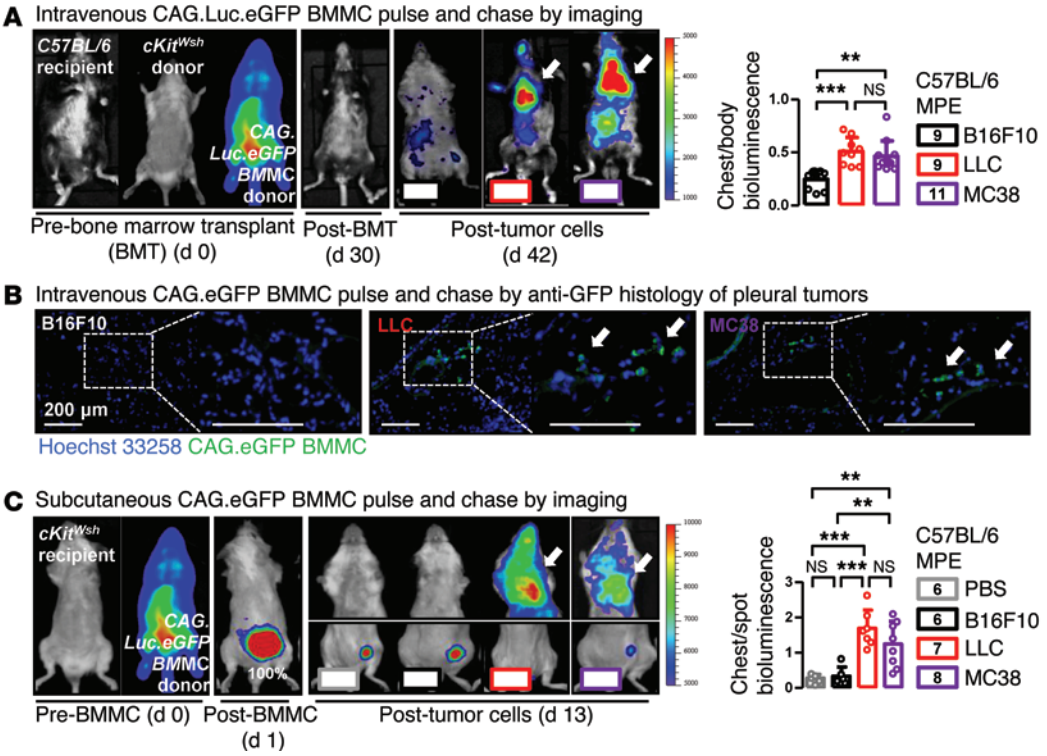

Figure 5. Dynamic MC trafficking to the pleural space. (**A**) Bioluminescence of C57BL/6 chimeras engrafted with *c-Kit*^{Wsh} BM that received 1.5 × 10^5 pleural B16F10 (n = 9), LLC (n = 9), or MC38 (n = 11) tumor cells and same-day i.v. 5 × 10^5 *CAG-luc-EGFP* BMMCs at day 30 after transplant. Note the increased chest signal in mice with adenocarcinoma-induced MPEs (arrows). (**B**) Pleural tumor sections (with magnified inlays) from chimeras as in (**A**) treated with pleural tumor cells followed by i.v. *CAG-EGFP* BMMCs (n = 5/group). Note GFP$^+$ BMMCs in adenocarcinomas 12 days later (arrows). (**C**) Bioluminescence of *c-Kit*^{Wsh} mice that received 8 x 10^5 s.c. *CAG-luc-EGFP* BMMCs followed by next-day pleural injections of PBS (n = 6) or B16F10 (n = 6), LLC (n = 7), or MC38 (n = 8) tumor cells. Note the increased chest signal in mice with adenocarcinomas 13 days later (arrows). Data presented as data points, mean ± SD. Numbers in boxes indicate sample size. NS, $P > 0.05$; $^{**}P < 0.01$; and $^{***}P < 0.001$, by 1-way ANOVA with Bonferroni post hoc tests.

c-Kit^{Wsh} or *Il1b*$^{-/-}$ — BMMCs could restore effusion formation (Figure 11, G and H). Both rmIL-1β and BMMC-CM selectively enhanced LLC and MC38 adenocarcinomas, but not B16F10 melanoma proliferation, in vitro (Figure 11I). rmIL-1β did not induce skin vessel leakage in C57BL/6 mice; on the contrary, rm tryptase AB1 (TPSAB1) did not affect cell proliferation (data not shown), but induced marked vascular hyperpermeability comparable to rmVEGF (Figure 11J). These results indicated that c-KIT–competent MCs facilitate MPE development by secreting TPSAB1 and IL-1β to foster vascular permeability and tumor growth, respectively.

MC-derived IL-1β activates NF-κB in pleural adenocarcinoma cells. NF-κB responds to IL-1α in cancer cells (45) and augments tumor growth and MPEs (46, 47). To test whether MC-derived products activate NF-κB and other important transcription pathways of tumor cells, such as STAT3 and NOTCH, we assessed the expression of 12 target genes of the above pathways by qPCR before and after 4 hours of treatment with BMMC-CM. Interestingly, none of the 12 genes examined was inducible by BMMC-CM in MPE-defective B16F10 cells; however, both NF-κB–target gene *Ccl2* and STAT3-target gene *Myc* were strongly upregulated by BMMC-CM selectively in MPE-competent adenocarcinoma cells (Figure 12A). By imaging a NF-κB reporter (p*NF-κB-Luc*; refs. 47, 48) and by immunoblotting, IL-1β (and IL-1α) and BMMC coculture induced and/or sustained NF-κB in adenocarcinoma, but not in B16F10 cells; this phenomenon was curtailed when *Il1b*$^{-/-}$ BMMCs were used and affected multiple NF-κB–pathway components (Figure 12, B–D, and Figure 13; full, uncut gels can be found in Supplemental Figures). In addition, *Il1r1* mRNA was selectively expressed by adenocarcinoma, but not B16F10 cells (Figure 12E and Supplemental Table 1). In vivo imaging of C57BL/6 and *c-Kit*^{Wsh} mice with pleural LLC cells expressing p*NF-κB-Luc* or a constitutive p*CAG-Luc* reporter verified that MC deficiency diminished tumor-specific NF-κB activation (Figure 14A). We next overexpressed *Ikbkb* (encoding IκB kinase [IKK] β), the main NF-κB–inducing kinase (45), in adenocarcinoma cells (Figure 14B). *Ikbkb*-overexpressing LLC cells were autonomous from IL-1β for NF-κB activation and equally caused MPEs in C57BL/6, *c-Kit*^{Wsh}, and *Cpa3*$^{Cre/+}$ mice (Figure 14, C and D), indicating that MC-elaborated IL-1β promotes MPEs by activating tumor cell IKKβ, thereby possibly establishing a positive feedback loop of enhanced MC recruitment by augmented tumor cell secretion of CCL2.

MC-mediated MPEs are actionable. To investigate whether the proposed pathway is targetable, we used c-KIT inhibitor imatinib mesylate (IM), which is clinically available. IM showed beneficial effects toward limiting LLC-induced effusions, and at the same time hampering pleural MC accumulation and vascular leakiness, when given at physiologically relevant once-daily doses of 1 mg/kg (Figure 15A). We also tested IM in the only

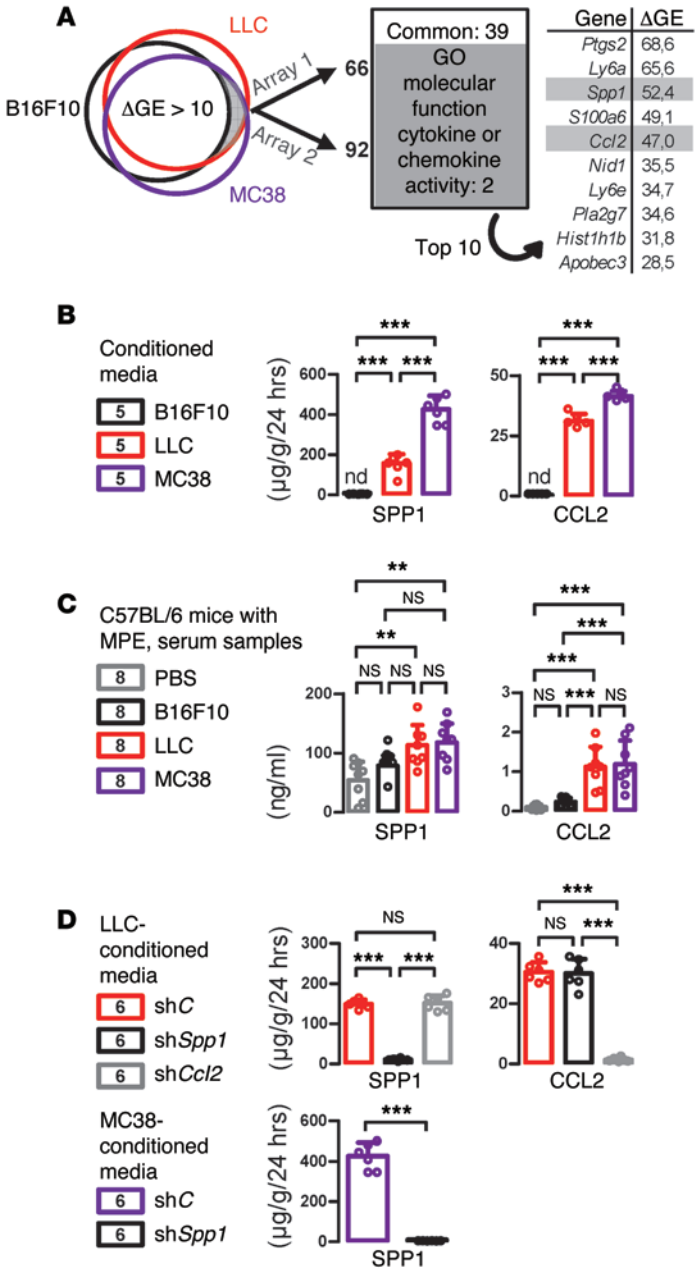

Figure 6. Identification of SPP1 and CCL2 as candidate tumor-derived MC effectors. (**A**) Venn diagram of mouse cancer cell differential gene expression (ΔGE) assessed by 2 microarrays showing 39 transcripts overrepresented in adenocarcinomas (top 10 listed), including *Ccl2* and *Spp1* (biological $n = 3$). (**B**) SPP1 and CCL2 ELISA of cancer cells–CM. (**C**) SPP1 and CCL2 ELISA of C57BL/6 mouse sera at day 14 after pleural PBS or cancer cells. (**D**) SPP1 and CCL2 ELISA of CM from LLC cells stably expressing random (shC), anti-*Spp1* (sh*Spp1*), or anti-*Ccl2* (sh*Ccl2*) shRNA, and MC38 cells stably expressing sh*C* or sh*Spp1*. Data represent 1 representative of 2 experiments and are presented as data points, mean ± SD. Numbers in boxes indicate the sample size. nd, not detected; NS, $P > 0.05$; $^{**}P < 0.01$; and $^{***}P < 0.001$, by 1-way ANOVA with Bonferroni post hoc tests.

available mouse model of MPEs caused by human cancer cells (38); A549 lung adenocarcinoma, but not SKMEL2 melanoma cells, elaborated SPP1/CCL2 and selectively caused MPE and MC accumulation upon pleural inoculation into *NOD/SCID* mice (Figure 15B). In addition, A549-induced MPEs were responsive to IM regression treatment (1 mg/kg daily) initiated on day 15 after establishment of pleural tumors (Figure 15C). Moreover, human MPEs from our biobank contained significantly elevated IL-1β levels compared with matched sera, a phenomenon not observed when CHF or IL-1α levels were examined (Figure 15D). In summary, our present work shows that MCs are required for MPEs, attracted to and activated in the pleural space by CCL2 and SPP1 of tumor cell origin. Once in the pleura, MCs secrete TPSAB1 and IL-1β to foster a hyperpermeable microenvironment and tumor NF-κB activation, respectively (Figure 15E).

Discussion

Here we report a connection between inflammation and cancer: MCs feed the inflammatory pleural environment fostering MPEs. We consistently found MCs in MPEs of patients and mice, and identified a plausible reason for their previous neglect. We also investigated MC trafficking and determined that these BM cells (49, 50) stream into the pleural cavities primarily attracted by tumor-originated CCL2. MCs were required for MPEs, since *c-Kit*^{Wsh} and *Cpa3*$^{Cre/+}$ mice were protected from adenocarcinoma-induced effusions and adoptive transfer of WT BM, as well as MC reconstitution, reinstalled MPEs in protected *c-Kit*^{Wsh} and *Il1b*$^{-/-}$ mice. c-KIT signaling was necessary for mastopoiesis and/or MC maintenance, since *c-Kit*^{Wsh} mice had reduced BMMC yield and decreased MC-like cells (29) in MPEs. Hence, it was shown here that c-KIT–intact MCs are essential for MPE

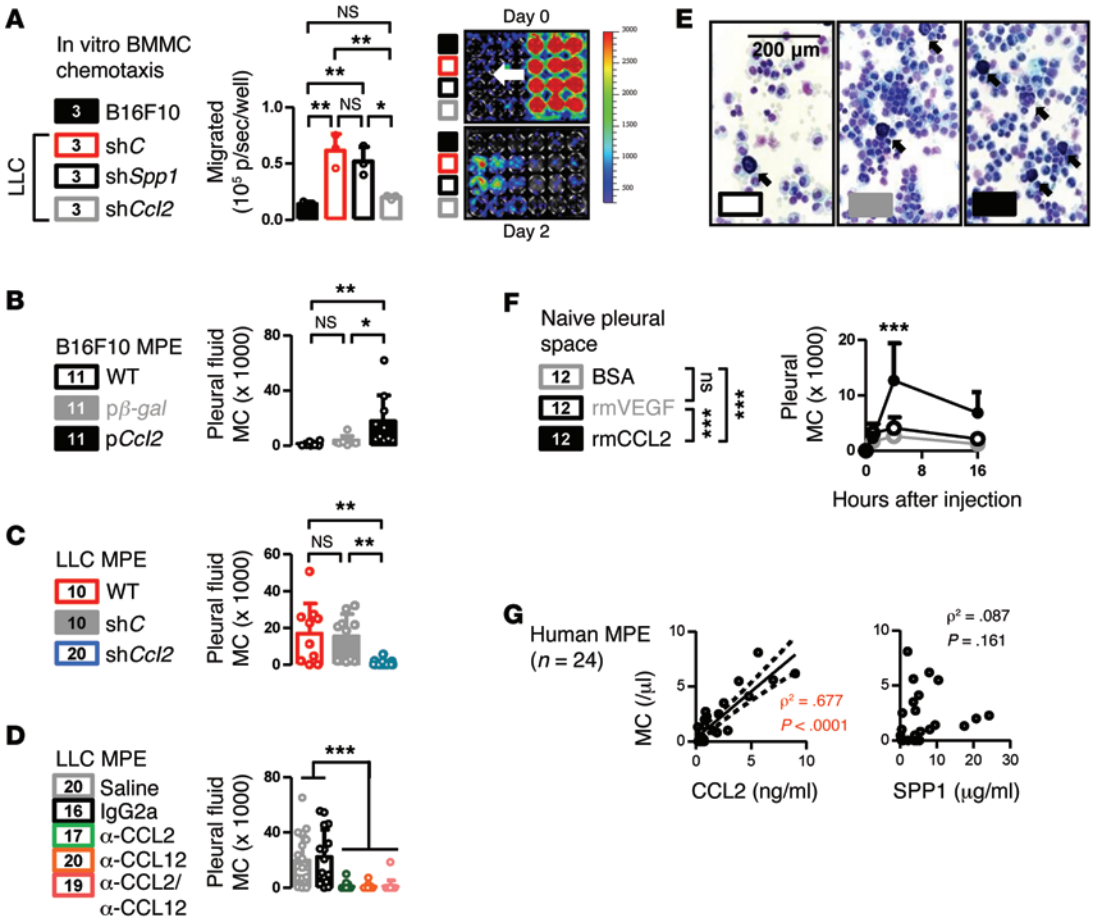

Figure 7. CCL2 is a tumor-derived mastokine. (**A**) Summary and images of 1 representative of 3 bioluminescent mastotaxis assays. Inserts carrying *CAG-luc-EGFP* BMMCs were transferred (arrow) onto wells containing B16F10 or LLC cells expressing sh*C*, sh*Spp1*, or sh*Ccl2* (n = 3/group) and were discarded after 2 days for imaging of transmigrated BMMCs. (**B**) Pleural MCs of C57BL/6 mice at day 14 after pleural *wt, β-gal,* or *Ccl2* plasmid (p*Ccl2*)-expressing B16F10 cells (n = 11/group). (**C**) Pleural MCs of C57BL/6 mice at day 14 after pleural delivery of WT (n = 10), sh*C* (n = 10), or sh*Ccl2*-expressing (n = 20) LLC cells. (**D**) Pleural MC accumulation of C57BL/6 mice at day 14 after pleural LLC cells was inhibited by CCL2 neutralization. Mice were treated with saline (n = 20), IgG (n = 16), or CCL2- (n = 17), CCL12- (n = 20), or both- (n = 19) neutralizing Ab (α) every 3 days after establishment of LLC cells. (**E** and **F**) Pleural MC (arrows) of C57BL/6 mice after pleural delivery of 30 ng BSA, rm VEGF, or rmCCL2 (n = 12/group). (**G**) CCL2 and SPP1 ELISA versus MC abundance of human MPEs from Figure 1A (n = 24) with linear regression line (95% CI), squared Spearman's correlation coefficients (ρ^2), and probability values (P). (**A**–**D**) Data presented as data points, mean ± SD. Numbers in boxes indicate sample size. nd, not detected; NS, $P > 0.05$; *$P < 0.05$; **$P < 0.01$; and ***$P < 0.001$, by 1-way (**A**–**D**) or 2-way (**F**) ANOVA with Bonferroni post hoc tests.

development. Moreover, it was shown that this less prevalent cellular population is as important for effusion formation as predominant immune cells such as macrophages.

Our data support that substantial populations of MCs exist in MPEs of humans and mice, and that they play a functional tumor-promoting role in the pleural space when the latter is taken over by metastatic tumors. This protumor role of pleural MCs appears to be conditional on the pleural space, since MCs were tumor-indifferent or even exerted antitumor functions in other tumor models (6, 12). The marked effusion-promoting effects of pleural-accrued MCs may be explained by the vast abundance of MCs in serosal cavities, a preferential site for their isolation (15). However, it is also conceivable that MCs, potent inflammatory regulators and vasoactors (51, 52), impact effusion formation more heavily than other tumor models, since MPE is mainly caused by inflammation and vasoactive signaling, and since the pleural cavities feature an extensive vascular bed (23, 24). Indeed, MCs secreted multiple inflammatory and vasoactive mediators upon adenocarcinoma encounter: histamine, a known permeability factor (9); TPSAB1 shown here to induce strong vasoactive effects; and IL-1β, a well-known NF-κB stimulus (45). Interestingly, the intrapleural levels of MC-originated TPSAB1 identified here may be responsible for the clinically well-known failure of normal, benign, and malignant pleural fluid to spontaneously coagulate, since TPSAB1 was recently found to cleave fibrinogen (53). Hence, tumor site likely determines MC function in cancer, and the pleural space probably constitutes a preferential theater for deployment of protumor MC effects.

Regardless of the tumor milieu, only certain tumor cells were able to initiate bidirectional signaling with MCs in our hands. First, only tumor cells competent of CCL2 secretion were able to attract substantial numbers of MCs to the pleural cavities. The finding of CCL2 as a cardinal MPE mastokine corrob-

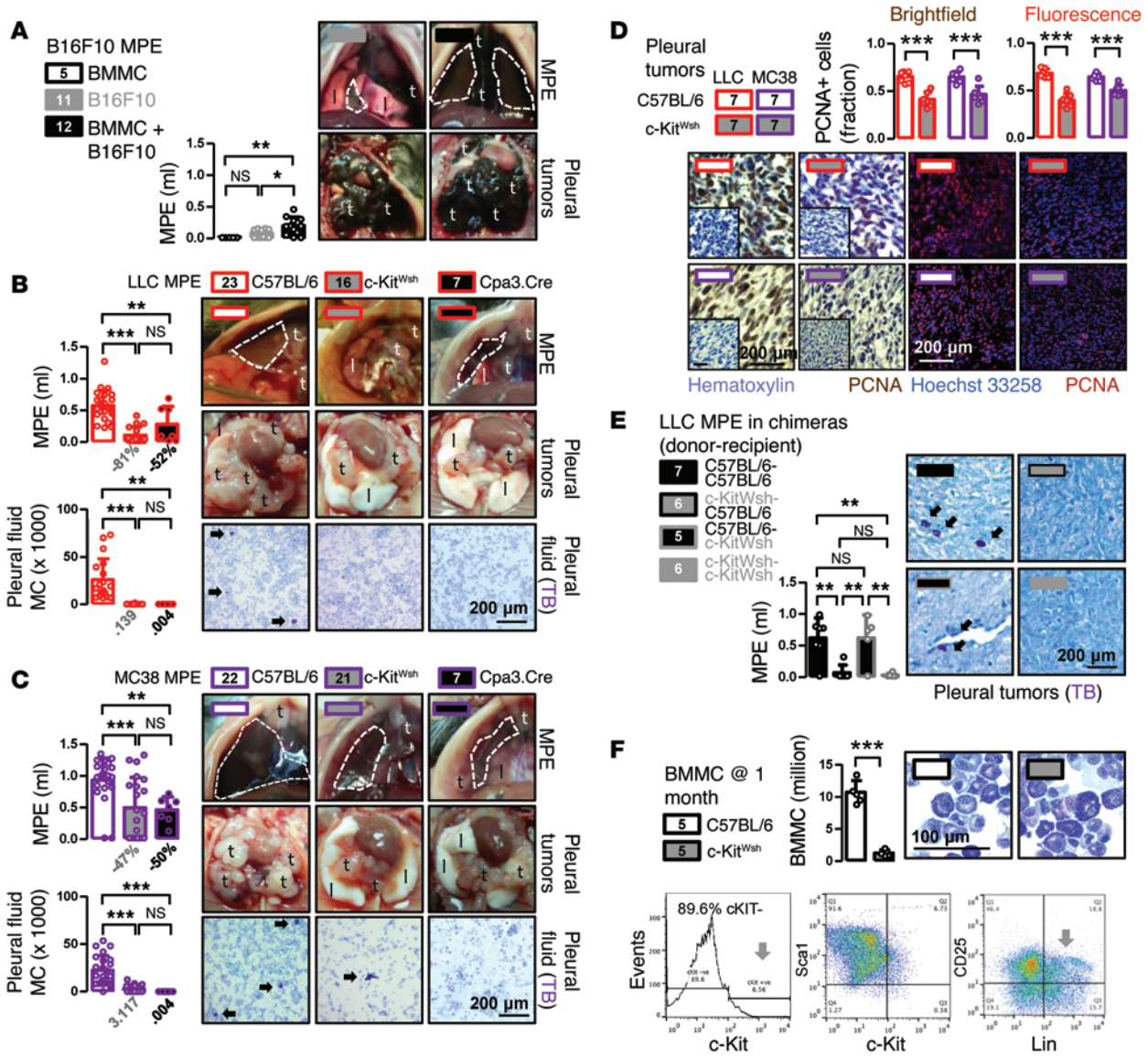

Figure 8. MCs are required for MPEs. (**A**) MPEs and pleural tumors of C57BL/6 mice at day 14 after pleural BMMCs (n = 5), B16F10 cells (n = 11), or both (n = 12). (**B** and **C**) MPEs, pleural tumors, and TB-stained pleural fluid cells including MCs of C57BL/6 (n = 45), *c-Kit*^{Wsh} (n = 37), and *Cpa3*$^{Cre/+}$ (n = 14) mice at day 14 after pleural LLC (**B**) and MC38 (**C**) cells. (**D**) PCNA immunoreactivity of pleural tumors from **B** and **C** (n = 7/group). (**E**) MPEs (graph) and TB-stained pleural tumor MCs (images) of irradiated C57BL/6 and *c-Kit*^{Wsh} recipients of BM transplants from C57BL/6 and *c-Kit*^{Wsh} donors at day 14 after pleural LLC cells (n = 6–7/group). (**F**) BMMC yield of C57BL/6 and *c-Kit*^{Wsh} mice (n = 6 each) at 1 month; data summary, TB-staining, and flow cytometry of *c-Kit*^{Wsh} BMMCs. Arrows indicate shift toward c-KIT$^-$Lin$^+$ phenotype, as compared with Figure 4B. Shown throughout are MPEs (dashed lines), lungs (l), pleural tumors (t), and MCs (arrows). Numbers below columns: percentile MPE inhibition and pleural MCs (thousands) of *c-Kit*^{Wsh} (gray font) and *Cpa3*$^{Cre/+}$ (black font) mice. Data presented as data points, mean ± SD. Numbers in boxes indicate sample size. NS, $P > 0.05$; *$P < 0.05$; **$P < 0.01$; and ***$P < 0.001$, by 2-tailed Student's t-test (**D**) or 1-way ANOVA with Bonferroni post hoc tests (all other graphs).

orates and expands work that identified CCL2 as the culprit for MC accrual to pancreatic tumors (6, 7). However, CCL2-mediated MC recruitment was not enough for full-blown tumor-MC interactions during MPE development; murine adenocarcinoma cells also secreted SPP1 that facilitated MC degranulation. On the contrary, B16F10 cells were unable to activate codelivered BMMCs, thus failing to mount full effusion-inducing properties, since they were found not to express SPP1. Finally, adenocarcinomas were selectively responsive to MC-originated IL-1β and expressed *Il1r1*, while melanoma cells did not. Taken together, our data suggest that MPE-prone adenocarcinomas may initiate circuitry with MCs due to coordinated expression of MC chemoattractants (i.e., CCL2) and effectors (i.e., SPP1), as well as the cognate receptors of MC-originated ligands such as IL-1β. The reason behind the propensity of the adenocarcinoma cells studied here to initiate crosstalk with MCs remains to be determined but can explain, together with the site-specificity discussed above, the differential impact of MCs on different tumors. In addition, these results can serve as a paradigm of how tumor-associated inflammatory cells can conditionally

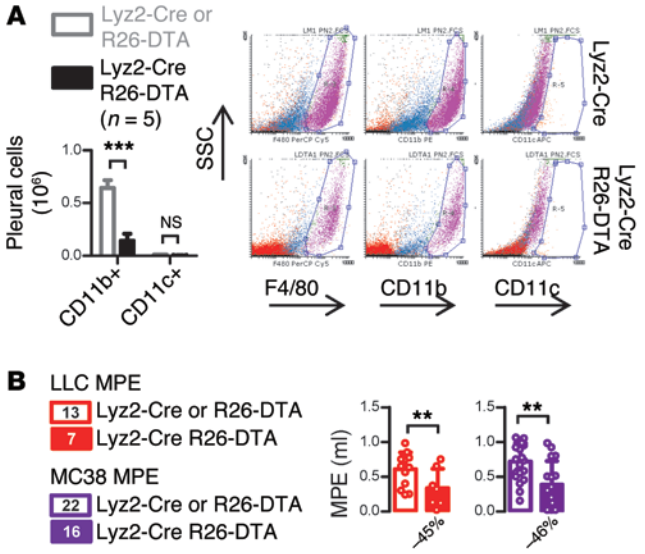

Figure 9. MC effects on MPEs parallel those of macrophages. (**A**) Flow cytometry gating and data summary of pleural cells from *Lyz2-Cre* or *R26-DTA* single transgenic controls, as well as *Lyz2-Cre R26-DTA* macrophage-deficient mice. Data presented as mean ± SD (n = 5/group). (**B**) MPEs of *Lyz2-Cre or R26-DTA* single transgenic controls (n = 35), as well as *Lyz2-Cre R26-DTA* macrophage-deficient mice (n = 23) at day 14 after pleural LLC (n = 20) or MC38 (n = 38) cells. Numbers below columns indicate percentile MPE inhibition of *Lyz2-Cre R26-DTA* mice. Data presented as data points, mean ± SD. Numbers in boxes indicate sample size. NS, $P > 0.05$; $^{**}P < 0.01$; and $^{***}P < 0.001$, by 2-tailed Student's t test.

modulate metastatic disease.

NF-κB integrates inflammatory stimuli from the tumor microenvironment to pivotally influence tumor cell survival and paracrine inflammatory signaling (54). In turn, immune cells stimulate tumor NF-κB, reinforcing a "vicious cycle" between tumor progression and inflammation (5, 55). NF-κB affects MPE progression, stimulated by tumor- and host-originated ligands of an ever-expanding cellular origin (26, 47, 48). Here we show that MC-secreted IL-1β upregulates NF-κB and cellular proliferation of pleural adenocarcinomas. Using in vivo imaging, we show in real time how MCs fuel tumor cell NF-κB and identify that IKKβ relies on MC-derived IL-1β to sustain the transcription factor. These findings are consistent with the recently reported *Nlrp3*-mediated IL-1β release by skin MCs (56), and they also strengthen the link between inflammation and cancer by positioning MCs as "feeder cells" of oncogenic NF-κB, as well as other important tumor cell transcription factors, such as STAT3 (57).

Importantly, the requirement for MCs during MPE development was actionable. Encouraging benefits were obtained from imatinib treatment of mice with syngeneic effusions, and concordant findings were recapitulated in human cancer cell–induced MPEs. These data strengthen the proposed connection and show how MC-targeted therapies can impact nongastrointestinal stromal tumors. The finding of significantly increased MCs and IL-1β in human MPEs compared with both matched serum samples and corresponding samples from patients with CHF suggests that our findings may be applicable to humans with established or impending MPEs, a possibility worth exploring.

In conclusion, we identified the conditional initiation and execution of a circuitry of tumor-initiated, MC-perpetuated inflammatory signaling events that occur during MPE formation. We show how tumor cells co-opt MCs to drive effusion development. In addition to the surprising discovery of MCs as culprits of MPEs, we identify CCL2, SPP1, TPSAB1, IL-1β, and IKKβ as key players in tumor cell–MC interactions in the pleural space. MCs per se, as well as each of the above targets, may present candidates for annihilating the requirement for MCs during MPE formation.

Methods

Further information can be found in Supplemental Methods.

Reagents. CCL2 and CCL12 neutralizing and IgG2a control Abs (37) were a gift from Oncology Discovery Research, Janssen Research & Development LLC. rmCCL2 was from Peprotech; rmIL-1β, rm IL-3, and rmKITL were from Immunotools; rmSPP1 and rmTPSAB1 were from R&D Systems; C48/80 and Evans' blue were from Sigma-Aldrich; ELISA kits were from Peprotech and R&D Systems; IM was from Selleckchem; and Boyden chambers were from Millipore.

Cells. LLC, B16F10, A549, and SKMEL2 (NCI) and MC38 cells (a gift from Barbara Fingleton, Vanderbilt University, Nashville, Tennessee, USA) (38) were cultured and tested as described in the Supplemental Methods. In vivo injections are described elsewhere (25, 26, 38, 47, 48). BM cells were flushed from femurs and tibias and cultured in full DMEM with rmIL-3 ± rmKITL (100 ng/ml each). Nonadherent cells were passaged for 4–6 weeks (31).

Animals. C57BL/6, *c-Kit*^{Wsh}, *NOD/SCID*, *CAG-luc-EGFP*, *CAG-EGFP*, *mT/mG*, *Lyz2-Cre* (39), and *R26-DTA* (40) mice (The Jackson Laboratory); *Cpa3*$^{Cre/+}$ mice (a gift from Hans-Reimer Rodewald, Heidelberg, Germany) (15); and *Il1b*$^{-/-}$ mice (a gift from Yoichiro Iwakura, Tokyo University of Science, Tokyo, Japan) (44) were bred at the Center for Animal Models of Disease of the University of Patras. Experiments were approved a priori by the local Veterinary Administration and were conducted according to 2010/63/EU. Experimental mice and littermate controls were sex-matched, weight-matched (20–25 g), and age-matched (6-12 weeks). For MPE generation, mice received 150,000 murine or 1,000,000 human cancer cells intrapleurally and were sacrificed after 14 or 30 days, respectively (38). IM (1 mg/kg) was given daily i.p. Anti–mouse CCL2 and CCL12 (a murine CCL2 ortholog) and IgG2a control Abs were delivered i.p. at 50 mg/kg every 3 days (37, 38). Harvest and pleural lavage are described elsewhere (25, 26, 38, 47, 48).

Humans. Pleural fluid was obtained during diagnostic thoracenteses in patients with MPEs (due to lung cancer [n = 14], breast cancer [n = 6], and malignant pleural mesothelioma [n = 4]) or CHF treated at General Hospital Evangelismos between 2006 and 2008. Samples from Hospital G. Papanikolaou were diagnostic MPE cyto-

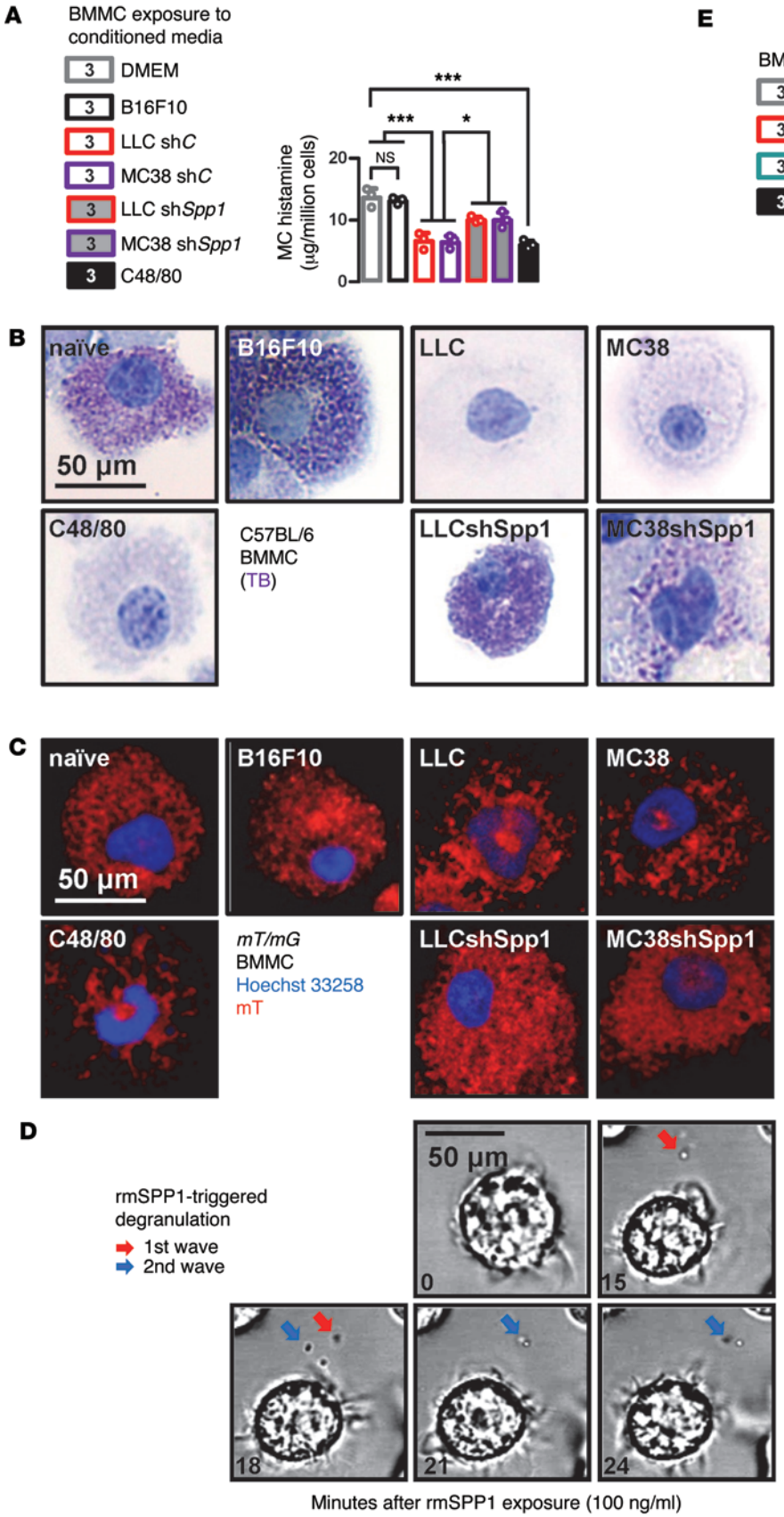

Figure 10. Tumor-secreted osteopontin causes MC degranulation. (**A**) Histamine content of C57BL/6 BMMCs after 2-hour incubation with indicated CM or C48/80 compound (potent MC degranulating compound used as positive control, *n* = 3/group). Note the partial effect of osteopontin silencing (sh*Spp1*), indicating that additional tumor-elaborated factors degranulate MCs. (**B** and **C**) C57BL/6 (**B**) and *mT/mG* (**C**) BMMC morphology after 2-hour incubation with indicated CM or C48/80 compound indicates that osteopontin is, at least in part, responsible for MC activation. (**D**) Time-lapse phase-contrast images of C57BL/6 BMMCs after direct exposure to rm SPP1 showing 2 consecutive waves of granule ejection (arrows). See also Supplemental Video 3. (**E**) C57BL/6 BMMC histamine content after 4-hour incubation with indicated rm mediators or C48/80 compound (*n* = 3/group) shows direct MC activation by osteopontin, which is only partial compared with C48/80. Data shown represent 1 representative of 3 experiments and are presented as data points, mean ± SD. Numbers in boxes indicate sample size. nd, not detected; NS, $P > 0.05$; *$P < 0.05$; and ***$P < 0.001$, by 1-way ANOVA with Bonferroni post hoc tests.

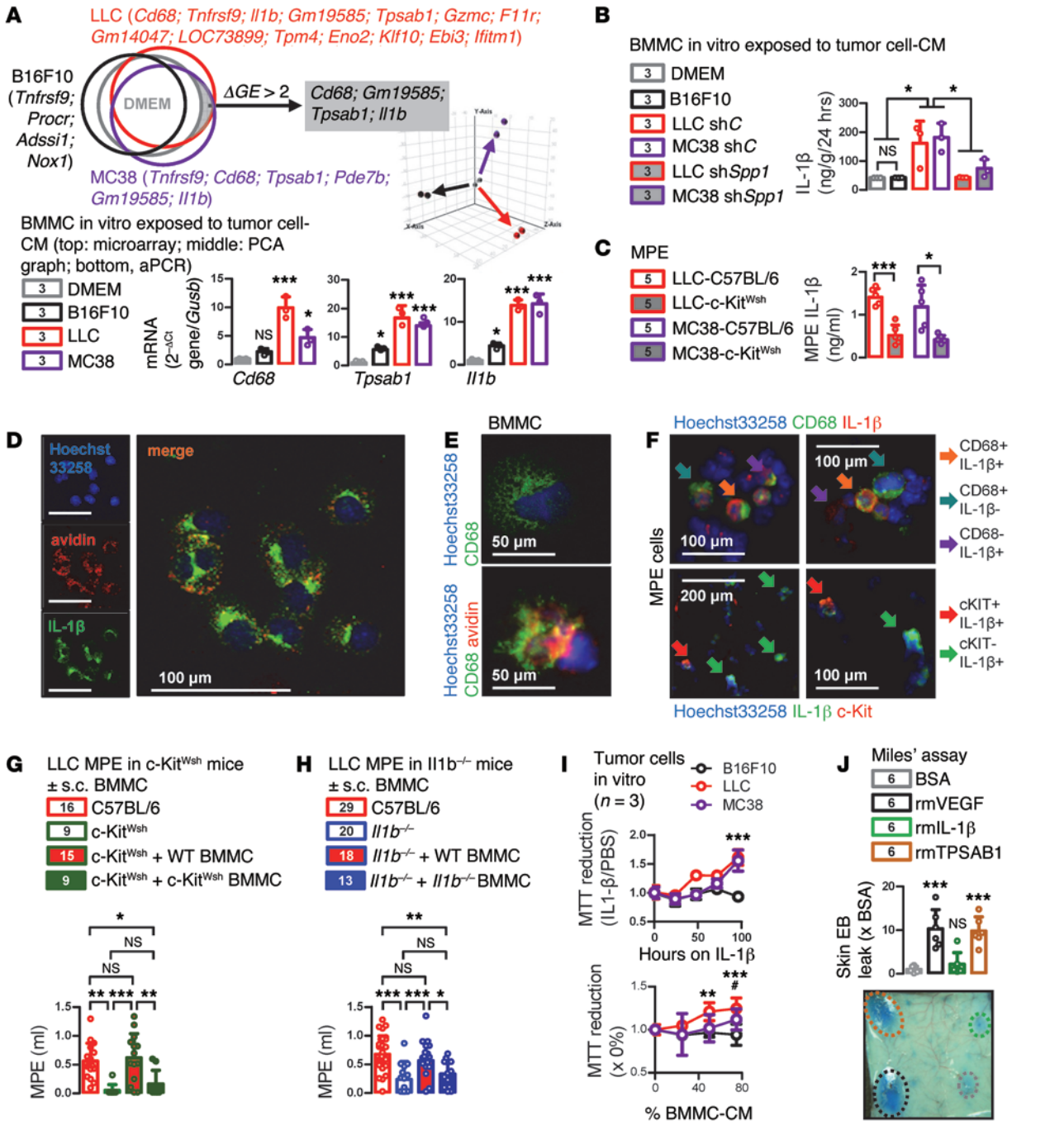

Figure 11. Adenocarcinoma-primed MCs secrete TPSAB1 and IL-1β. (**A**) Microarray (Venn and PCA diagrams, $n = 2$) and qPCR ($n = 3$) of BMMC differential gene expression (ΔGE) after tumor-CM exposure. Comparisons with naive BMMCs. (**B**) C57BL/6 BMMC-CM IL-1β ELISA after 4 hours of sham or tumor-CM exposure ($n = 3$/treatment). (**C**) MPE IL-1β ELISA of mice from Figure 8, B and C ($n = 5$/group). (**D** and **E**) IL-1β (**D**) and CD68 (**E**) immunolocalization in C57BL/6 BMMCs counterstained with Hoechst 33258 (nuclei) and avidin (granules). (**F**) IL-1β colocalization with c-KIT and CD68 in MPE cells. (**G** and **H**) MPEs of C57BL/6 ($n = 45$), *c-Kit*^{Wsh} (**G**, $n = 33$), and *Il1b*$^{-/-}$ (**H**, $n = 51$) mice 14 days after pleural LLC cells with or without s.c. C57BL/6, *c-Kit*^{Wsh}, or *Il1b*$^{-/-}$ BMMCs. (**I**) Proliferation of B16F10, LLC, and MC38 cells ($n = 3$/cell line) at 100 ng/ml IL-1β (top; comparisons of adenocarcinomas with melanoma) and at increasing BMMC-CM concentrations (bottom; comparisons of LLC [stars] and MC38 [number sign] cells with 0% BMMC-CM [control]). (**J**) C57BL/6 skin Evans' blue leak (color-coded areas) induced by BSA or rm cytokines (comparisons with BSA, $n = 6$/group). (**A**, **B**, and **I**) Shown are 1 representative of 3 experiments. Data are presented as data points, mean ± SD. Numbers in boxes indicate sample size. NS, $P > 0.05$; $^*P < 0.05$; $^{**}P < 0.01$; and $^{***}P < 0.001$, by 2-way (**I**) or 1-way (all other graphs) ANOVA with Bonferroni post hoc tests.

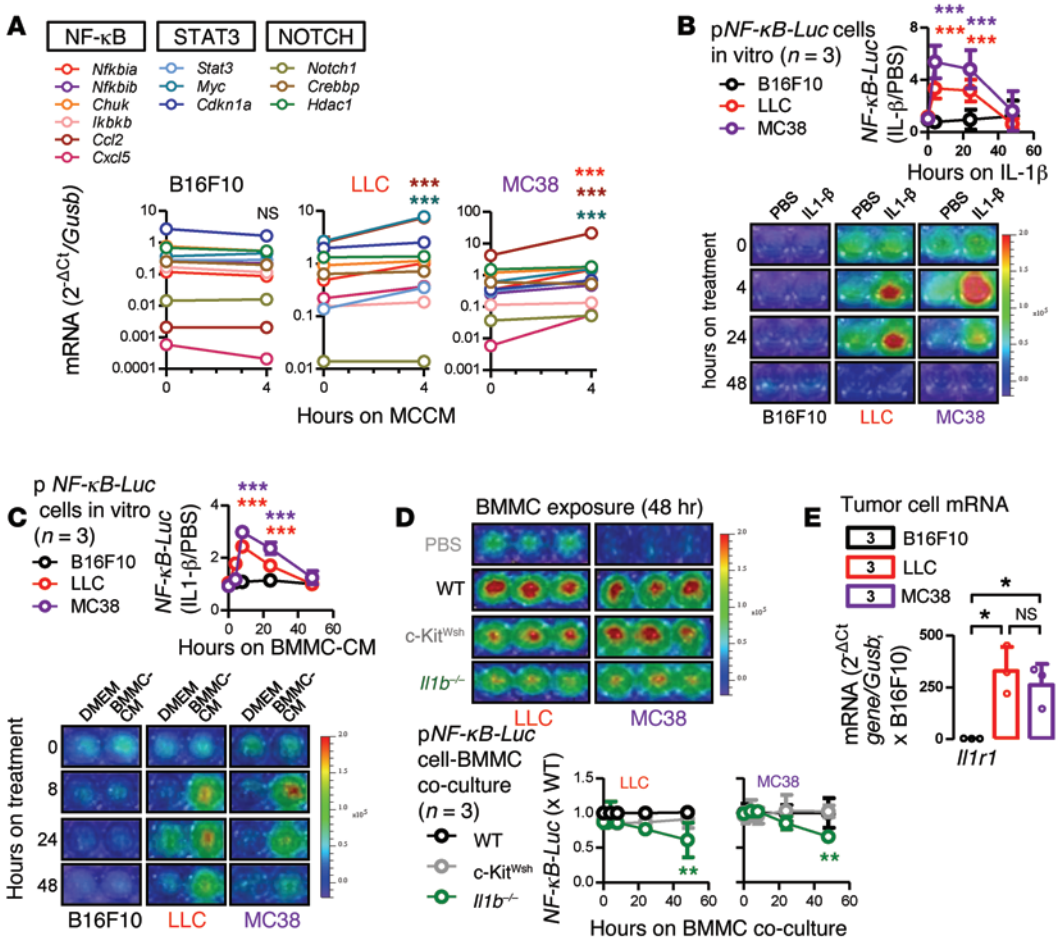

Figure 12. MC-derived IL-1β activates NF-κB in adenocarcinoma cells. (**A**) Tumor cell mRNA expression levels by qPCR of 12 target genes of the NF-κB, STAT3, and NOTCH pathways before and 4 hours after exposure to BMMC-CM. *n* = 3/data point. (**B** and **C**) Cancer cell NF-κB reporter (p*NF-κB-Luc*) activity induced by rmIL-1β (**B**) and BMMC-CM (**C**). *n* = 3/data point. (**D**) Tumor cell p*NF-κB-Luc* activity induced by C57BL/6, *c-Kit*^{Wsh}, or *Il1b*$^{-/-}$ BMMC coculture. *n* = 3/data point. (**E**) *Il1r1* qPCR of tumor cell RNA. *n* = 3/data point. Significance indicators stand for comparison of color-matched data at indicated time-point compared with baseline (**A**), B16F10 cells (**B** and **C**) or with C57BL/6 BMMC (**D**). Shown is 1 representative of 3 experiments. Data presented as mean ± SD (**A**–**D**) or data points, mean ± SD (**E**). Numbers in boxes indicate sample size. NS, $P > 0.05$; *$P < 0.05$; **$P < 0.01$; and ***$P < 0.001$, by 1-way (**E**) or 2-way (all other graphs) ANOVA with Bonferroni post hoc tests.

logic specimens from 20 patients with lung adenocarcinoma aspirated in 2013. Diagnosis and sample handling are described elsewhere (25, 26, 48). All protocols abided by the Helsinki Declaration were approved a priori by the relevant IRB and by all patients via written informed consent.

Cytology and histology. Cell and tissue specimens, prepared as described in the Supplemental Methods, were stained with MGG, TB (0.05%; 5–15 minutes), or the indicated Abs (Supplemental Table 6) and counterstained with hematoxylin, Hoechst 33258 (Sigma-Aldrich; dilution 1:5000), Envision (Dako), and/or avidin (Vector Laboratories). MCs were counted as a percentage of 10,000 cells on cytology or of all cells on histology. Microscopy was done on an AxioObserver D1 (Zeiss) or an SP5 (Leica Microsystems) microscopes.

Flow cytometry. After NH_4Cl red blood cell lysis, cells were suspended in PBS 2% FBS, stained with the indicated Abs (Supplemental Table 6) for 20 minutes, fixed in 1% paraformaldehyde (10 minutes), and analyzed on a FACSCalibur (BD Biosciences). Data were examined using FlowJo.

Constructs. Random (shC), anti-*Ccl2* (sh*Ccl2*), or anti-*Spp1* (sh*Spp1*) shRNAs, as well as *Ccl2* and *β-gal* expression vectors, have been described (25, 41). p*EGFP* and p*EGFP.Ikbkb* (Addgene IDs 58249 and 58251) were cloned from MC38 total RNA using specific primers (Supplemental Table 7). Cells were transfected with 5 μg DNA by X-fect reagent (BD Biosciences — Clontech) and selected by puromycin.

BM cell transfer. For adoptive BM replacement (Figure 5, A and B, and Figure 8E), mice received 10 million BM cells i.v. 12 hours after total-body irradiation (1100 Rad; ref. 35). For MC pulse and chase (Figure 5), irradiated C57BL/6 chimeras engrafted with *c-Kit*^{Wsh} BM (39) received pleural tumor cells at day 30 after transplant, followed by same-day 5×10^5 i.v. *CAG-luc-EGFP* or *CAG-EGFP* BMMCs; nonirradiated *c-Kit*^{Wsh} mice received 8×10^5 s.c. *CAG-luc-EGFP* BMMCs, followed by next-day pleural tumor cells. For intrapleural BMMC delivery (Figure 8A), C57BL/6 mice received 10^5 intrapleural BMMCs, with or without B16F10 cells. For BMMC give-back (Figure 11, G and H), 2.5×10^5 BMMC were administered s.c.

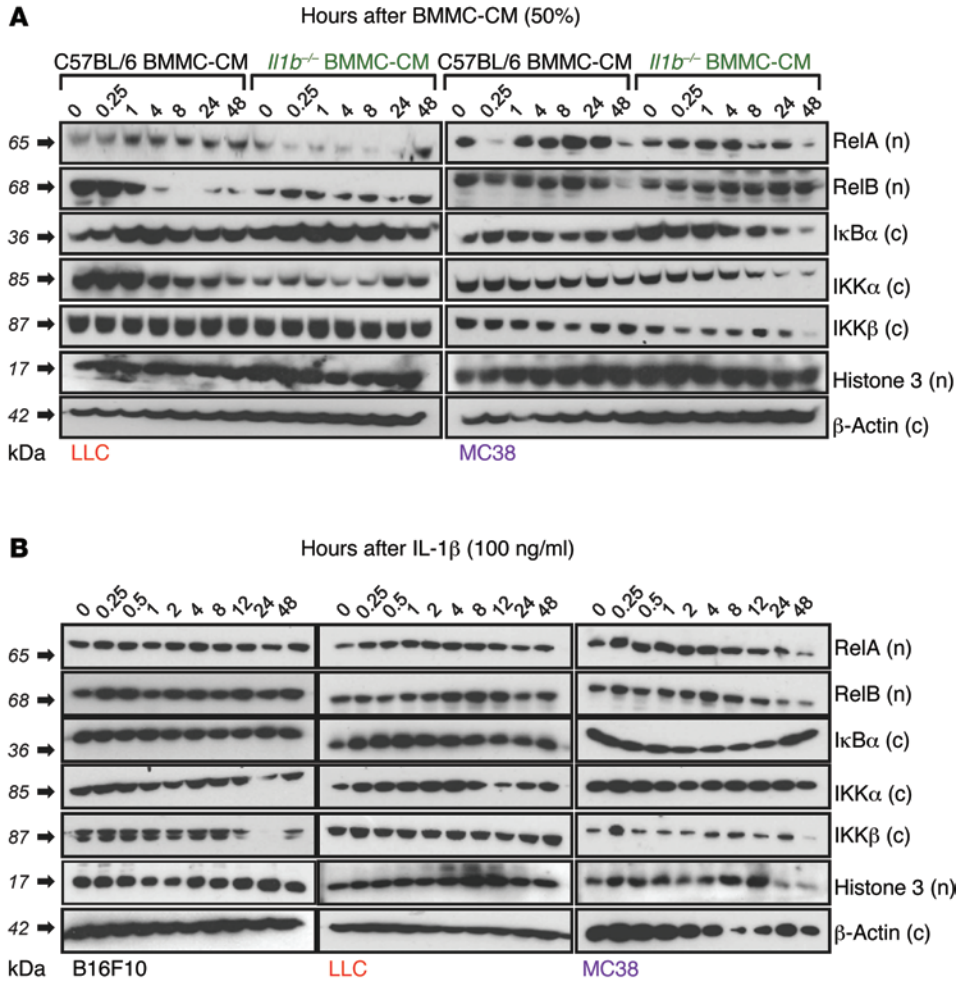

Figure 13. Tumor cell NF-κB subunit profiling after exposure to MC-coditioned media and IL-1β. Immunoblots of cytoplasmic (c) and nuclear (n) tumor cell extracts for NF-κB pathway components after C57BL/6 or *Il1b*$^{-/-}$ BMMC-CM exposure (**A**) or treatment with 100 ng/ml rmIL-1β (**B**).

Bioluminescence imaging. Cells and mice were imaged after the addition of 300 μg/ml D-luciferin to culture media or i.v. delivery of 1 mg D-luciferin on a Xenogen Lumina II. Data were analyzed on Living Image v.4.2 (PerkinElmer) (47, 48).

Vascular permeability assays. Mice with MPEs received 0.8 mg Evans' blue i.v. and were killed after 1 hour for determination of MPE levels of the albumin tracer (48). Intradermal injections of test molecules (1.5 ng/50 μl PBS), cell-free MPEs (50 μl), or cancer cell–conditioned media (50 μl) were followed by Evans' blue injection as above, and euthanasia, skin inversion and imaging after 1 hour (25). Dye leak was determined using Fiji (http://fiji.sc/Fiji).

qPCR and microarray. RNA was isolated using Trizol (Invitrogen) followed by RNAeasy (QIAGEN), RNA was reverse transcribed using Superscript III (Invitrogen), and reverse transcriptase or qPCR was performed using specific primers (Supplemental Table 7). For microarray, 5 μg RNA pooled from triplicate samples was tested for quality, labeled, and hybridized to GeneChip Mouse Gene 1.0 or 2.0 ST arrays (Affymetrix). Data (http://www.ncbi.nlm.nih.gov/geo/; Accession ID: GSE58190) were analyzed as detailed in the Supplemental Methods.

Immunoblotting. Nuclear and cytoplasmic extracts were prepared using NE-PER (Thermo), separated by 10% SDS-PAGE, and electroblotted to PVDF membranes (Millipore). Membranes were probed with specific Ab (Supplemental Table 6), and were visualized by enhanced chemiluminescence.

Cellular assays. Tumor cell proliferation in response to IL-1β or BMMC-CM was determined using MTT reduction (Promega). MC migration was studied in Boyden chambers with 8.0 μm pores (36): cancer cells were cultured in the lower and bioluminescent BMMCs in the upper chambers. After 48 hours, the upper chambers were removed and the bioluminescent signal of transmigrated BMMCs was measured by imaging. MC histamine was measured by the o-phthalaldehyde method (58). All cellular experiments were done at least 3 times, while 1 representative experiment is shown.

Statistics. Sample size was calculated using G*power (http://www.gpower.hhu.de/; ref. 59) assuming $\alpha = 0.05$, $\beta = 0.8$, and $\rho = 0.3$. No data were excluded. Animals were allocated to treatments by alternation, and transgenic animals were enrolled case-control–wise. Data acquisition was blinded on samples previously coded by a nonblinded investigator. All data were examined for normality by Kolmogorov-Smirnof test. Values are given as mean ± SD and median ± interquartile range, as indicated. Sample size (n) refers to biological replicates. Differences in means were examined by

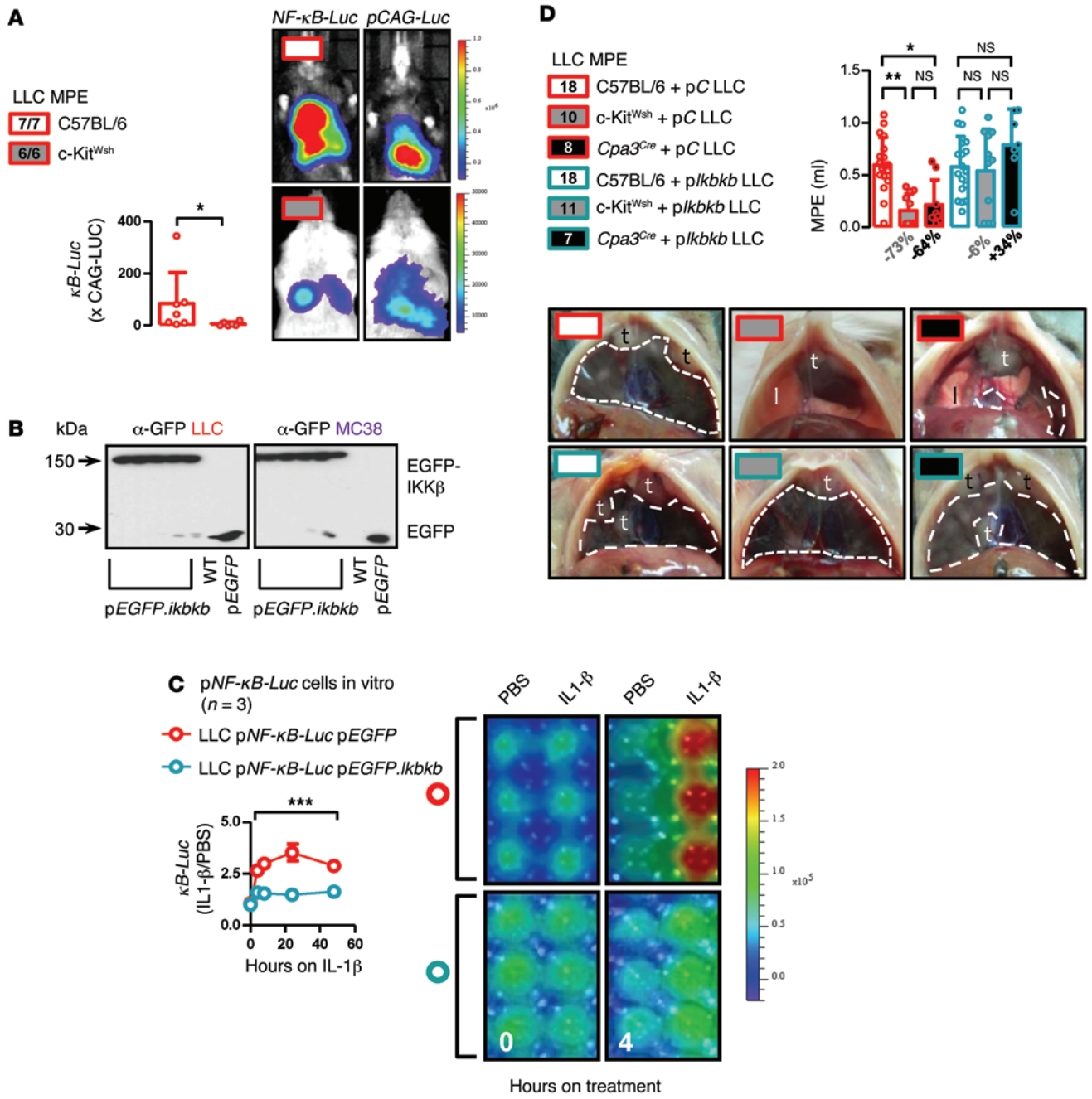

Figure 14. MC-derived IL-1β promotes effusion development via IκB kinase (IKK) β. (**A**) Bioluminescence of C57BL/6 (n = 14) and *c-Kit*^{Wsh} (n = 12) mice 14 days after pleural LLC cells expressing constitutive (p*CAG-Luc*) or NF-κB-dependent (p*NF-κB-Luc*) reporters. (**B**) Validation of adenocarcinoma cells overexpressing p*EGFP* and p*EGFP.Ikbkb*. (**C**) Bioluminescence of p*NF-κB-Luc* LLC cells expressing p*EGFP* or p*EGFP.Ikbkb* in response to 100 ng/ml IL-1β, with comparisons of p*EGFP.Ikbkb* with p*EGFP* cells (n = 3/data-point). Shown is 1 representative of 3 experiments. (**D**) MPEs of C57BL/6 (n = 36), *c-Kit*^{Wsh} (n = 21), and *Cpa3*$^{Cre/+}$ (n = 15) mice 14 days after pleural p*EGFP*- or p*EGFP.Ikbkb*-expressing LLC cells. Shown are MPEs (dashed lines), lungs (l), and pleural tumors (t). Numbers below columns indicate percentile MPE inhibition of *c-Kit*^{Wsh} (gray font) and *Cpa3*$^{Cre/+}$ (black font) mice. Data presented as data points, mean ± SD. Numbers in boxes indicate sample size. NS, $P > 0.05$; *$P < 0.05$; **$P < 0.01$; and ***$P < 0.001$, by Student's t test (**A**), 1-way (**D**), or 2-way (**C**) ANOVA with Bonferroni post hoc tests.

2-tailed Student's t test, or 1-way or 2-way ANOVA with Bonferroni post-tests, as appropriate, and in medians by Mann-Whitney U test or Kruskal-Wallis test with Dunn's post hoc tests. Correlations were done using Pearson's r or Spearman's ρ. P values are 2-tailed, and $P < 0.05$ was considered significant. Analyses and plots were done on Prism v5.0 (GraphPad Software).

Study approval. All animal experiments were approved a priori by the Veterinary Administration of Western Greece according to a full and detailed protocol (approval 276134/14873/2). Human studies were approved a priori by the Ethics Committee of the General Hospital of Athens Evangelismos (Athens, Greece; approval 379-7/12/2006 and extension 323-4/12/2012).

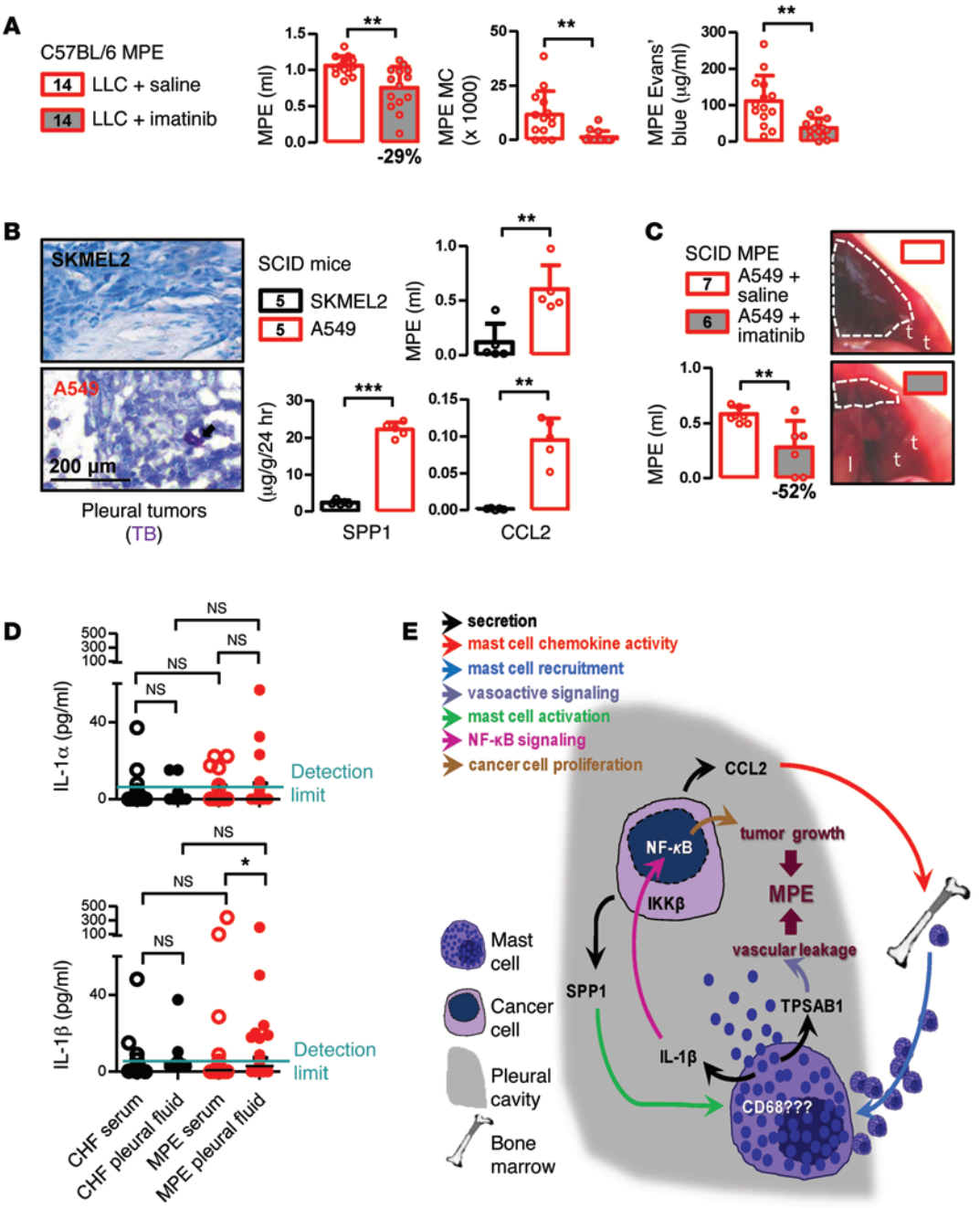

Figure 15. MC-mediated MPEs are actionable in mice and humans. (**A**) MPEs, MPE MCs, and Evans' blue content after i.v. delivery of 0.8 mg of the dye of C57BL/6 mice at day 14 after pleural delivery of 1.5×10^5 LLC cells and daily treatment with intraperitoneal PBS or IM, as indicated (n = 14/group). Percentage indicates IM-mediated MPE inhibition. (**B**) MCs in pleural tumors (arrows) and MPE volume of *NOD/SCID* mice 30 days after pleural human cancer cells, and SPP1/CCL2 ELISA of human tumor cell–CM (n = 5/group). (**C**) A549-induced MPEs of *NOD/SCID* mice at day 30 after establishment of A549 cells, after treatment with PBS (n = 7) or IM (n = 6) starting at day 15 after establishment of A549 cells. Shown are MPEs (dashed lines), lungs (l), and pleural tumors (t). Percentage indicates IM-mediated MPE inhibition. (**D**) Pleural and serum IL-1α/β of patients with CHF (n = 26) and MPEs (n = 24) from Figure 1A. (**E**) Graphical summary of present work: pleural adenocarcinomas secrete CCL2 and SPP1, which facilitate, respectively, pleural MC accumulation and activation. Upon tumor cell encounter, MCs release TPSAB1 and IL-1β, which increase vascular leakage and tumor NF-κB activation, respectively. Data presented as data points and median ± interquartile range (**D**) or mean ± SD (all other graphs). Cytokine measurements in (**B**) were repeated 3 times; shown are data from 1 experiment. Numbers in boxes indicate sample size. NS, $P > 0.05$; $^*P < 0.05$; $^{**}P < 0.01$; and $^{***}P < 0.001$, by Student's t test (**A**–**C**) or Kruskal-Wallis ANOVA with Dunn's post hoc tests (**D**).

Acknowledgments

This work was supported by European Research Council 2010 Starting Independent (260524 to G.T. Stathopoulos) and 2009 Advanced (233074 to H.R. Rodewald) Investigator Grants, by a Hellenic Thoracic Society 2012 Research Award (to A.D. Giannou and G.T. Stathopoulos), by European Respiratory Society 2009 Maurizio Vignola and 2013 Romain Pauwels Research Awards (to G.T. Stathopoulos), by a 2013 European Respiratory Society Long Term Research Fellowship (1824 to I. Psallidas), by a Thorax Foundation (Athens, Greece) 2006 Fellowship (to G.T. Stathopoulos), by US NIH (HL61419) and VA Merit Review Grants (to T.S. Blackwell), and by Ruprecht-Karls-University Heidelberg SFB 938 Project L (to H.R. Rodewald). The authors thank the University of Patras Center for Animal Models of Disease and Advanced Light Microscopy Core for experimental support, Panagiota Stamou and Alexandros Spiridonidis for flow cytometry support, Charis Roussos and Androniki Kollintza for insightful discussions, and Georgia Papaspyrou for editorial assistance.

Address correspondence to: Georgios T. Stathopoulos or Antonia Marazioti, Faculty of Medicine, University of Patras, 1 Asklepiou Street, University Campus, 26504 Rio, Greece. Phone: 30.2610.969154; E-mail: gstathop@upatras.gr (G.T. Stathopoulos); amarazioti@upatras.gr (A. Marazioti).

1. Hanahan D, Weinberg RA. Hallmarks of cancer: the next generation. *Cell*. 2011;144(5):646–674.
2. Swamy M, Jamora C, Havran W, Hayday A. Epithelial decision makers: in search of the 'epimmunome'. *Nat Immunol*. 2010;11(8):656–665.
3. Coussens LM, Pollard JW. Leukocytes in mammary development and cancer. *Cold Spring Harb Perspect Biol*. 2011;3(3):a003285.
4. Floor SL, Dumont JE, Maenhaut C, Raspe E. Hallmarks of cancer: of all cancer cells, all the time? *Trends Mol Med*. 2012;18(9):509–515.
5. Balkwill FR, Mantovani A. Cancer-related inflammation: common themes and therapeutic opportunities. *Semin Cancer Biol*. 2012;22(1):33–40.
6. Soucek L, Lawlor ER, Soto D, Shchors K, Swigart LB, Evan GI. Mast cells are required for angiogenesis and macroscopic expansion of Myc-induced pancreatic islet tumors. *Nat Med*. 2007;13(10):1211–1218.
7. Theoharides TC. Mast cells and pancreatic cancer. *N Engl J Med*. 2008;358(17):1860–1861.
8. Galli SJ, Kalesnikoff J, Grimbaldeston MA, Piliponsky AM, Williams CM, Tsai M. Mast cells as "tunable" effector and immunoregulatory cells: recent advances. *Annu Rev Immunol*. 2005;23:749–786.
9. Theoharides TC, Kempuraj D, Tagen M, Conti P, Kalogeromitros D. Differential release of mast cell mediators and the pathogenesis of inflammation. *Immunol Rev*. 2007;217:65–78.
10. Chen R, et al. Mast cells play a key role in neutrophil recruitment in experimental bullous pemphigoid. *J Clin Invest*. 2001;108(8):1151–1158.
11. Blair RJ, et al. Human mast cells stimulate vascular tube formation. Tryptase is a novel, potent angiogenic factor. *J Clin Invest*. 1997;99(11):2691–2700.
12. Sinnamon MJ, Carter KJ, Sims LP, Lafleur B, Fingleton B, Matrisian LM. A protective role of mast cells in intestinal tumorigenesis. *Carcinogenesis*. 2008;29(4):880–886.
13. Dalton DK, Noelle RJ. The roles of mast cells in anticancer immunity. *Cancer Immunol Immunother*. 2012;61(9):1511–1520.
14. Pittoni P, Colombo MP. The dark side of mast cell-targeted therapy in prostate cancer. *Cancer Res*. 2012;72(4):831–835.
15. Feyerabend TB, et al. Cre-mediated cell ablation contests mast cell contribution in models of antibody- and T cell-mediated autoimmunity. *Immunity*. 2011;35(5):832–844.
16. Dudeck A, et al. Mast cells are key promoters of contact allergy that mediate the adjuvant effects of haptens. *Immunity*. 2011;34(6):973–984.
17. Roberts ME, Neville E, Berrisford RG, Antunes G, Ali NJ. Management of a malignant pleural effusion: British Thoracic Society Pleural Disease Guideline 2010. *Thorax*. 2010; 65(suppl 2):ii32–ii40.
18. Ryu JS, et al. Prognostic impact of minimal pleural effusion in non-small-cell lung cancer. *J Clin Oncol*. 2014;32(9):960–967.
19. Burgers JA, Kunst PW, Koolen MG, Willems LN, Burgers JS, van den Heuvel M. Pleural drainage and pleurodesis: implementation of guidelines in four hospitals. *Eur Respir J*. 2008;32(5):1321–1327.
20. Davies HE, Lee YC. Management of malignant pleural effusions: questions that need answers. *Curr Opin Pulm Med*. 2013;19(4):374–379.
21. Postmus PE, et al. The IASLC Lung Cancer Staging Project: proposals for revision of the M descriptors in the forthcoming (seventh) edition of the TNM classification of lung cancer. *J Thorac Oncol*. 2007;2(8):686–693.
22. Wu SG, et al. Survival of lung adenocarcinoma patients with malignant pleural effusion. *Eur Respir J*. 2013;41(6):1409–1418.
23. Stathopoulos GT, Kalomenidis I. Malignant pleural effusion: tumor-host interactions unleashed. *Am J Respir Crit Care Med*. 2012;186(6):487–492.
24. Marazioti A, Blackwell TS, Stathopoulos GT. The lymphatic system in malignant pleural effusion. Drain or immune switch? *Am J Respir Crit Care Med*. 2014;189(6):626–627.
25. Stathopoulos GT, et al. A central role for tumor-derived monocyte chemoattractant protein-1 in malignant pleural effusion. *J Natl Cancer Inst*. 2008;100(20):1464–1476.
26. Stathopoulos GT, et al. Host derived interleukin-5 promotes adenocarcinoma-induced malignantpleural effusion. *Am J Respir Crit Care Med*. 2010;182(10):1273–1281.
27. Murdoch C, Muthana M, Coffelt SB, Lewis CE. The role of myeloid cells in the promotion of tumour angiogenesis. *Nat Rev Cancer*. 2008;8(8):618–631.
28. Ema H, et al. Adult mouse hematopoietic stem cells: purification and single-cell assays. *Nat Protoc*. 2006;1(6):2979–2987.
29. Brickshawana A, Shapiro VS, Kita H, Pease LR. Lineage(–)Sca1+c-Kit(–)CD25+ cells are IL-33-responsive type 2 innate cells in the mouse bone marrow. *J Immunol*. 2011;187(11):5795–5804.
30. Tono T, et al. c-kit Gene was not transcribed in cultured mast cells of mast cell-deficient Wsh/Wsh mice that have a normal number of erythrocytes and a normal c-kit coding region. *Blood*. 1992;80(6):1448–1453.
31. Okayama Y, Kawakami T. Development, migration, and survival of mast cells. *Immunol Res*. 2006;34(2):97–115.
32. Muzumdar MD, Tasic B, Miyamichi K, Li L, Luo L. A global double-fluorescent Cre reporter mouse. *Genesis*. 2007;45(9):593–605.
33. Cao YA, et al. Shifting foci of hematopoiesis during reconstitution from single stem cells. *Proc Natl Acad Sci U S A*. 2004;101(1):221–226.
34. Okabe M, Ikawa M, Kominami K, Nakanishi T, Nishimune Y. 'Green mice' as a source of ubiquitous green cells. *FEBS Lett*. 1997;407(3):313–319.
35. Chen J, et al. Adoptive transfer of syngeneic bone marrow-derived cells in mice with obesity-induced diabetes: selenoorganic antioxidant ebselen restores stem cell competence. *Am J Pathol*. 2009;174(2):701–711.
36. Kitaura J, et al. IgE– and IgE+Ag-mediated mast cell migration in an autocrine/paracrine fashion. *Blood*. 2005;105(8):3222–3229.
37. Tsui P, et al. Generation, characterization and biological activity of CCL2 (MCP-1/JE) and CCL12 (MCP-5) specific antibodies. *Hum Antibodies*. 2007;16(3-4):117–125.
38. Marazioti A, et al. Beneficial impact of CCL2 and CCL12 neutralization on experimental malignant pleural effusion. *PLoS One*. 2013;8(8):e71207.
39. Wolters PJ, et al. Tissue-selective mast cell reconstitution and differential lung gene expression in mast cell-deficient Kit(W-sh)/Kit(W-sh) sash mice. *Clin Exp Allergy*. 2005;35(1):82–88.
40. Yamazaki M, et al. C-kit gene is expressed by skin mast cells in embryos but not in puppies of Wsh/Wsh mice: age-dependent abolishment of c-kit gene expression. *Blood*. 1994;83(12):3509–3516.
41. Clausen BE, Burkhardt C, Reith W, Renkawitz R, Förster I. Conditional gene targeting in macrophages and granulocytes using LysMcre mice. *Transgenic Res*. 1999;8(4):265–277.
42. Voehringer D, Liang HE, Locksley RM. Homeostasis and effector function of lymphopenia-induced "memory-like" T cells in constitutively T cell-depleted mice. *J Immunol*. 2008;180(7):4742–4753.
43. Psallidas I, et al. Secreted phosphoprotein-1 directly provokes vascular leakage to fos-

ter malignant pleural effusion. *Oncogene*. 2013;32(4):528–535.
44. Horai R, et al. Production of mice deficient in genes for interleukin (IL)-1α, IL-1β, IL-1α/β, and IL-1 receptor antagonist shows that IL-1β is crucial in turpentine-induced fever development and glucocorticoid secretion. *J Exp Med*. 1998;187(9):1463–1475.
45. Ling J, et al. KrasG12D-induced IKK2/β/NF-κB activation by IL-1α and p62 feedforward loops is required for development of pancreatic ductal adenocarcinoma. *Cancer Cell*. 2012;21(1):105–120.
46. Greten FR, et al. IKKβ links inflammation and tumorigenesis in a mouse model of colitis-associated cancer. *Cell*. 2004;118(3):285–296.
47. Stathopoulos GT, et al. Nuclear factor-κB affects tumor progression in a mouse model of malignant pleural effusion. *Am J Respir Cell Mol Biol*. 2006;34(2):142–150.
48. Stathopoulos GT, et al. Tumor necrosis factor-α promotes malignant pleural effusion. *Cancer Res*. 2007;67(20):9825–9834.
49. Chen CC, Grimbaldeston MA, Tsai M, Weissman IL, Galli SJ. Identification of mast cell progenitors in adult mice. *Proc Natl Acad Sci U S A*. 2005;102(32):11408–11413.
50. Maaninka K, Lappalainen J, Kovanen PT. Human mast cells arise from a common circulating progenitor. *J Allergy Clin Immunol*. 2013;132(2):463–469.
51. Zhang Y, Ramos BF, Jakschik BA. Augmentation of reverse arthus reaction by mast cells in mice. *J Clin Invest*. 1991;88(3):841–846.
52. Tilley SL, Wagoner VA, Salvatore CA, Jacobson MA, Koller BH. Adenosine and inosine increase cutaneous vasopermeability by activating A(3) receptors on mast cells. *J Clin Invest*. 2000;105(3):361–367.
53. Prieto-García A, et al. Mast cell restricted mouse and human tryptase·heparin complexes hinder thrombin-induced coagulation of plasma and the generation of fibrin by proteolytically destroying fibrinogen. *J Biol Chem*. 2012;287(11):7834–7844.
54. DiDonato JA, Mercurio F, Karin M. NF-κB and the link between inflammation and cancer. *Immunol Rev*. 2012;246(1):379–400.
55. Dong G, Chen Z, Kato T, Van Waes C. The host environment promotes the constitutive activation of nuclear factor-κB and proinflammatory cytokine expression during metastatic tumor progression of murine squamous cell carcinoma. *Cancer Res*. 1999;59(14):3495–3504.
56. Nakamura Y, Franchi L, Kambe N, Meng G, Strober W, Núñez G. Critical role for mast cells in interleukin-1β-driven skin inflammation associated with an activating mutation in the nlrp3 protein. *Immunity*. 2012;37(1):85–95.
57. Yeh HH, Lai WW, Chen HH, Liu HS, Su WC. Autocrine IL-6-induced Stat3 activation contributes to the pathogenesis of lung adenocarcinoma and malignant pleural effusion. *Oncogene*. 2006;25(31):4300–4309.
58. Fujiwara M, Ishida Y, Nimura N, Toyama A, Kinoshita T. Postcolumn fluorometric detection system for liquid chromatographic analysis of amino and imino acids using o-phthalaldehyde/N-acetyl-L-cysteine reagent. *Anal Biochem*. 1987;166(1):72–78.
59. Faul F, Erdfelder E, Lang AG, Buchner A. G*Power 3: A flexible statistical power analysis program for the social, behavioral, and biomedical sciences. *Behavior Research Methods*. 2007;39(2):175–191.